


Recent trends in analysis of mycotoxins in food using carbon-based nanomaterials

Follow this and additional works at: <https://www.jfda-online.com/journal>

 Part of the [Food Science Commons](#), [Medicinal Chemistry and Pharmaceutics Commons](#), [Pharmacology Commons](#), and the [Toxicology Commons](#)



This work is licensed under a [Creative Commons Attribution-Noncommercial-No Derivative Works 4.0 License](#).

Recommended Citation

Chen, Bing-Huei and Inbaraj, Baskaran Stephen (2022) "Recent trends in analysis of mycotoxins in food using carbon-based nanomaterials," *Journal of Food and Drug Analysis*: Vol. 30 : Iss. 4 , Article 6.
Available at: <https://doi.org/10.38212/2224-6614.3437>

This Review Article is brought to you for free and open access by Journal of Food and Drug Analysis. It has been accepted for inclusion in Journal of Food and Drug Analysis by an authorized editor of Journal of Food and Drug Analysis.

Recent trends in analysis of mycotoxins in food using carbon-based nanomaterials

Bing-Huei Chen, Baskaran Stephen Inbaraj*

Department of Food Science, Fu Jen Catholic University, New Taipei City, 24205, Taiwan

Abstract

Mycotoxins (MYTs), a class of low molecular weight secondary metabolites produced by filamentous fungi in food and feed, pose serious global threat to both human health and world economy. Due to their mutagenic, teratogenic, carcinogenic and immunosuppressive effects, the International Agency for Research on Cancer has classified various MYTs under Group 1 to 3 category with aflatoxins being designated under Group 1 category (carcinogenic to humans). Also, the presence of MYTs in trace amounts in diverse food matrices necessitates exploration of highly sensitive methods for onsite analysis. Although conventional chromatographic methods are highly sensitive, they are expensive, tedious and cannot be applied for rapid onsite analysis. In recent years the application of nanomaterials especially carbon-based nanomaterials (CNMs) in the fabrication of low-cost and miniaturized electrochemical and optical sensors has enabled rapid onsite analysis of MYTs with high sensitivity and specificity. Moreover, the CNMs are employed as effective solid phase extraction (SPE) adsorbents possessing high specific surface area for effective enrichment of MYTs to improve the sensitivity of chromatographic methods for MYT analysis in food. This article aims to overview the recent trends in the application of CNMs as SPE adsorbents for sample pretreatment in chromatographic methods as well as in the fabrication of highly sensitive electrochemical and optical sensors for rapid analysis of MYTs in food. Initially, the efficiency of various functionalized CNMs developed recently as adsorbent in packed SPE cartridges and dispersive SPE adsorbent/purification powder is discussed. Then, their application in the development of various electrochemical immunosensors involving functionalized carbon nanotubes/nanofibers, graphene oxide, reduced graphene oxide and graphene quantum dots is summarized. In addition, the recent trends in the use of CNMs for fabrication of electrochemical and fluorescence aptasensors as well as some other colorimetry, fluorometry, surface-enhanced Raman spectroscopy and electrochemical based sensors are compared and tabulated. Collectively, this review article can provide a research update on analysis of MYTs by carbon-based nanomaterials paving a way for identifying future perspectives.

Keywords: Electrochemical immunosensor, Electrochemical aptasensor, Fluorescence aptasensor, Mycotoxin, SPE adsorbents

1. Introduction

Food safety is a vital health-related issue and many countries including Taiwan have established a law for critical control of food safety and sanitation with a main goal to achieve ultimate protection for human health [1,2]. Mycotoxins (MYTs) are a class of low molecular weight food toxins (300–700 Da) produced as secondary metabolites by fungi during pre- and post-harvest of various agricultural products including cereals, cereal-based foods, corn, rice, rye, wheat, barley, oats, sorghum, soybeans, buckwheat, peanut, malt, beer, dried

fruits, wine, milk, baby and infant foods, coffee beans, cocoa, bakery and meat products [2,3]. The MYTs are most commonly produced by filamentous fungi such as *Aspergillus*, *Fusarium* and *Penicillium* species with their levels increasing during storage under high temperature and humidity conditions [4]. The presence of MYTs in foods and feeds not only result in serious economic loss but also cause deleterious, acute and chronic effects on human health. The fungal source, occurrence in food/feed and their toxicity have been elaborately reported elsewhere [2,5]. Most importantly, the MYTs are not only carcinogenic, teratogenic, mutagenic and/or

Received 17 August 2022; accepted 31 August 2022.
Available online 23 November 2022

* Corresponding author.
E-mail addresses: sinbaraj@yahoo.com, 138547@mail.fju.edu.tw (B.S. Inbaraj).

<https://doi.org/10.38212/2224-6614.3437>

2224-6614/© 2022 Taiwan Food and Drug Administration. This is an open access article under the CC-BY-NC-ND license (<http://creativecommons.org/licenses/by-nc-nd/4.0/>).

hepatotoxic, but also affect the pulmonary, cardiovascular and central nervous systems [6,7].

Although about 300–400 MYTs are found in nature, only a few of them are important from the human health point of view and a list of MYTs classified by the International Agency for Research on Cancer [8–10] along with their abbreviation, chemical formula, molecular weight and IARC toxicity level is shown in Table 1. Among various MYTs, aflatoxins (AFB1, AFB2, AFG1, AFG2, AFM1 and AFM2) are highly toxic and classified as carcinogenic under Group 1 category [8]. In addition, ochratoxin A (OTA), ochratoxin B (OTB), fumonisin B1 (FB1), fumonisin B2 (FB2), sterigmatocystin (SMC) and fusarin C (FSC), belonging to Group 2B of IARC category have been demonstrated to be nephrotoxic and carcinogenic, mainly attributed to the DNA adduct formation and oxidative stress [2,7,11]. Consequently, the maximum permissible

limits (MPLs) of MYTs are established in over 100 countries by several organizations including European Union (EU) and United States Food and Drug Administration (USFDA) for MYTs in various food products. According to the European Commission (EC), the MPL for total AFs, AFB1, AFM1, OTA, fumonisin (FNs), zearalenone (ZEA) and deoxynivalenol (DON)/patulin (PAT) is 4, 2, 0.05, 2–10, 200–1000, 20–100, 200–500 ng/g, respectively, while USFDA has recommended similar MPLs with the exception of 20 ng/g for total AFs, 2000–4000 ng/g for FN and 1000 ng/g for DON [12–14]. In Taiwan, the MPL for total AFs is set at 15 ng/g for peanut and maize and 10 ng/g for other foods [2]. Thus, the development of a feasible and highly sensitive analytical method for detection of MYTs in food and feed is important.

Due to the presence of MYTs in low amounts in the complex matrices of food, their analysis has

Table 1. A list of mycotoxins based on IARC classification including those discussed in this review along with their abbreviation, chemical formula, molecular weight and IARC toxicity level.

No.	Name	Abbreviation	Chemical formula	Molecular weight	Toxicity (IARC) ^{a,b}
1	Aflatoxin B1	AFB1	C ₁₇ H ₁₂ O ₆	329.15	1
2	Aflatoxin B2	AFB2	C ₁₇ H ₁₄ O ₆	314.29	1
3	Aflatoxin G1	AFG1	C ₁₇ H ₁₂ O ₇	328.27	1
4	Aflatoxin G2	AFG2	C ₁₇ H ₁₄ O ₇	330.29	1
5	Aflatoxin M1	AFM1	C ₁₇ H ₁₂ O ₇	328.28	1
6	Aflatoxin M2	AFM2	C ₁₇ H ₁₄ O ₇	330.29	1
7	Ochratoxin A	OTA	C ₂₀ H ₁₈ ClNO ₆	403.81	2B
8	Ochratoxin B	OTB	C ₂₀ H ₁₉ NO ₆	369.40	2B
9	Fumonisin B1	FB1	C ₃₄ H ₅₉ NO ₁₅	721.83	2B
10	Fumonisin B2	FB2	C ₃₄ H ₅₉ NO ₁₄	739.58	2B
11	Sterigmatocystin	SMC	C ₁₈ H ₁₂ O ₆	324.30	2B
12	Fusarin C	FSC	C ₂₃ H ₂₉ NO ₇	431.50	2B
13	Deoxynivalenol	DON	C ₁₅ H ₂₀ O ₆	296.31	3
14	3-Acetyl deoxynivalenol	3ADON	C ₁₇ H ₂₂ O ₇	338.35	3
15	15-Acetyl deoxynivalenol	15ADON	C ₁₇ H ₂₂ O ₇	338.40	3
16	Zearalenone	ZEA	C ₁₈ H ₂₂ O ₅	318.36	3
17	Citrinin	CIT	C ₁₃ H ₁₄ O ₅	250.25	3
18	T-2	T-2	C ₂₄ H ₃₄ O ₉	466.50	3
19	HT-2	HT-2	C ₂₂ H ₃₂ O ₈	424.48	3
20	Fusarenone X	FSX	C ₁₇ H ₂₂ O ₈	354.40	3
21	Patulin	PAT	C ₇ H ₆ O ₄	154.12	3
22	Nivalenol	NIV	C ₁₅ H ₂₀ O ₇	312.30	3
23	Cyclochlorotine	CCT	C ₂₄ H ₃₁ Cl ₂ N ₅ O ₇	572.44	3
24	Kojic acid	KJA	C ₆ H ₆ O ₄	142.11	3
25	Luteoskyrin	LTS	C ₃₀ H ₂₂ O ₁₂	574.50	3
26	Penicillic acid	PCA	C ₇ H ₈ O ₃	170.16	3
27	Rugulosin	RGS	C ₃₀ H ₂₂ O ₁₀	542.50	3
28	Tenuazonic acid	TEA	C ₁₀ H ₁₅ NO ₃	197.23	—
29	Altenuene	ALT	C ₁₅ H ₁₆ O ₆	292.28	—
30	Tentoxin	TEN	C ₂₂ H ₃₀ N ₄ O ₄	414.50	—
31	Neosolaniol	NEO	C ₁₉ H ₂₆ O ₈	382.40	—
32	Mycophenolic acid	MPA	C ₂₃ H ₂₈ O ₁₂	496.50	—
33	Diacetoxyscripenol	DAS	C ₁₉ H ₂₆ O ₇	366.40	—
34	Alternariol	ALT	C ₁₄ H ₁₀ O ₅	258.23	—
35	Agroclavine	AGL	C ₁₆ H ₁₈ N ₂	238.33	—

^a Based on International Agency Research on Cancer.

^b Group 1, carcinogenic to human; Group 2B, possibly carcinogenic to human; Group 3, not classified as to carcinogenic to human.

been difficult. MYTs are often extracted with aqueous mixture of acetonitrile or methanol in the presence of salt, followed by employing clean-up methods such as solid-phase extraction (SPE) or antigen–antibody interaction-based immune-affinity column [14]. However, these methods are time consuming and the residual impurities can interfere with chromatographic analysis resulting in low recovery. For MYT analysis, most official methods are based on high-performance liquid chromatograph (HPLC) coupled with diode array, fluorescence or mass spectrometric detection, in which HPLC-tandem mass spectrometer (MS/MS) has been widely used for simultaneous determination of MYTs [14–16]. Also, the enzyme-linked immunosorbent assay (ELISA) has been successfully used for analyzing a large number of samples in a single run, especially with the quantitative ELISA kits and immunochromatography test kits, both of which enable rapid analysis of MYTs [14,17]. Some other emerging techniques such as fluorescence polarization assays and Fourier transform near-infrared spectroscopy as well as incorporation of recombinant antibody fragments and DNA aptamers as receptors have also been employed for high-throughput MYT analysis [2,14]. However, although these methods provide high sensitivity, they are expensive, time-consuming, laborious, requiring skilled personnel and incapable to perform onsite analysis.

Over the recent years, sensors have emerged as portable devices capable of analyzing target analytes by incorporating special recognition elements for precise measurement on an appropriate transducer [3,18,19]. Incorporation of nanotechnology in the construction of sensors has facilitated highly sensitive and selective analysis of toxins including MYTs. Due to their excellent optical, electrical, mechanical and catalytic properties, various classes of nanomaterials including metal/metal oxide nanoparticles, carbon nanomaterials (CNMs) and their nanocomposites have been explored in the design of sensors for enhancement of sensitivity and device miniaturization [4,20]. Of the various nanomaterials, CNMs have become promising materials for detection of MYTs as they possess unique characteristics including high specific surface area, biocompatibility, ease of functionalization and excellent electrical transmission ability [19,21,22]. Depending on the ratio of sp , sp^2 and sp^3 hybridization in CNMs, different types of CNMs are formed including graphene quantum dots (GQDs) (0D CNMs), carbon nanotubes (CNTs)/carbon nanofibers (CNFs) (1D CNMs) and graphene materials (2D CNMs) [4,22]. These CNMs exhibit remarkable surface properties

for functionalization with a variety of polymers/biomolecules/nanoparticles towards eventual immobilization of a large amount of recognition elements (antibody and aptamer) to improve detector response [3,23]. Moreover, they are often used alone or as nanocomposite with functional polymers or magnetic nanoparticles (Fe_3O_4) for application in SPE, dispersive SPE (dSPE) or QuEChERS (Quick, Easy, Cheap, Effective, Rugged and Safe) sample pretreatment enabling efficient magnetic separation and highly sensitive analysis of MYTs even in complex food matrices [10,24–26].

In the present review, recent trends in the application of CNMs for analysis of MYTs in food are summarized and tabulated, discussing specifically their application as SPE adsorbents coupled with liquid chromatographic methods as well as in the design of electrochemical immunosensors, electrochemical aptasensors, fluorescence aptasensors and other optical/electrochemical sensors. Various CNMs covered in this review include single-walled CNTs (SWCNTs), multi-walled CNTs (MWCNTs), CNFs, graphene (GR), graphene oxide (GO), reduced graphene oxide (rGO), GQDs, graphene oxide quantum dots (GOQDs) and their nanocomposites with polymers and metal/metal oxide nanoparticles.

2. Carbon nanomaterials as SPE adsorbents for MYT analysis by liquid chromatographic methods

2.1. Multi-walled carbon nanotubes-based SPE adsorbents

Owing to the presence of MYTs in complex mixture at ultralow levels, their extraction and pre-concentration are the critical steps associated with the quantitation of MYTs. The SPE with packed cartridges is one of the most commonly used clean-up procedures possessing several advantages including high enrichment factor, efficiency in eliminating interferences, rapid phase separation and less organic solvent/time consumption [27]. However, the application of commonly used liquid–liquid extraction and SPE using immunoaffinity columns is tedious and expensive, especially for the commercial SPE cartridges with high throughput screening of MYTs [14,28]. Both CNTs and GO-based adsorbents alone or in combination with magnetic iron oxide, polymer or metal nanoparticles have emerged to be promising SPE adsorbents for application as packing materials in SPE cartridge [24,29], dSPE adsorbents [26,30] and QuEChERS purification powders [10,25] in sample

pretreatment. Specifically, MWCNTs exhibit high adsorption capacity because of their unique electronic, mechanical, and chemical properties, i.e., their hollow and layered structure with abundant π -electrons, making them attractive as adsorbent materials for development of effective SPE-based sample pretreatment techniques [10,28]. In recent years, magnetic MWCNTs composed of magnetic Fe_3O_4 and MWCNTs has shown promising application as SPE adsorbents with specific advantages of easy surface modification, high surface area and rapid magnetic separation [24,29]. Table 2 summarizes the various MWCNTs-Carbon nanomaterial developed recently as SPE adsorbents for MYT analysis by liquid chromatographic methods.

A composite of Fe_3O_4 /MWCNTs synthesized by assembling Fe_3O_4 with MWCNTs using sonication through aggregation wrap mechanism was used as SPE adsorbent for extraction, purification and enrichment of ZEA and 4 type A trichothecenes including T-2 toxin, HT-2 toxin, neosolaniol and diacetoxyscirpenol in Danshen (*Salviae miltiorrhizae* Radix et Rhizoma) [29]. With the optimized SPE conditions of 2% aqueous acetonitrile as loading solution, 5% aqueous methanol as washing solution and 0.5% formic acid in acetone as elution solvent, a high sensitivity with the limit of detection (LOD) being 0.45–1.80 ng/g, limit of quantitation (LOQ) 1.20–4.80 ng/g, recovery 73.7–91.9%, relative standard deviation (RSD) of intraday precision 2.1–11.0% and RSD of interday precision 4.9–13.3% shown by using an ultra-HPLC-tandem mass spectrometer (UHPLC-MS/MS) method with a Poroshell EC-C18 column (100 \times 3.0 mm internal diameter (ID), particle size 2.7 μm) and a gradient mobile phase of water and methanol (1 mL/min) coupled with electrospray ionization detection in multiple reaction monitoring (MRM) mode.

Although the magnetic MWCNTs are successfully used as SPE adsorbents, the poor solubility and stability in aqueous medium hinder their application in complex matrices. To remedy this problem, the magnetic MWCNTs are recently modified with a water-soluble polymer like polyethylene glycol (PEG) or polyethyleneimine (PEI) prior to their use for sample pretreatment. For example, Zhao et al. [28] prepared PEGylated magnetic MWCNTs (PEG-MNPs@MWCNTs) with polyethylene glycol 2000 by adding 10 mg of PEG-MNPs@MWCNTs followed by 5-min vortex mixing, magnetic separation and desorption with 5 mL of 1% formic acid in ethyl acetate, a total of 13 MYTs were successfully isolated from milk. Analysis by UHPLC-High Resolution Mass Spectrometer (HRMS) showed a good linear response with high sensitivity (LOD,

0.005–0.050 ng/g; LOQ, 0.015–0.150 ng/g), acceptable recovery (81.8–106.4%) and high precision (intraday RSD, 2.1–8.5%; interday RSD, 3.9–11.7%) by using an Accucore aQ column (150 \times 2.1 mm ID, particle size 3.5 μm) and a gradient mobile phase of 0.1% formic acid in water and acetonitrile and HRMS detection using both positive and negative ionization in full scan mode. A much higher sensitivity in detection of 10 MYTs in milk (LOD, 0.003–0.442 ng/g; LOQ, 0.008–1.219 ng/g) was reported by Li et al. [26], who used PEI-modified and 3-glycidioxypropyltrimethoxysilane-linked magnetic MWCNTs (PEI-GPMS-MNPs@MWCNTs) with surface area, magnetization and adsorption capacity at 38.3 m^2/g , 65.2 emu/g and 4.9–10.2 mg/g, respectively. At an optimized dose of 20 mg, extraction time of 3 min, desorption time of 2 min and desorption solvent of 0.5% formic acid in methanol (5 mL), a high accuracy and precision was shown with the recovery ranging from 88.3 to 103.5% as well as the RSD for the intraday- and interday-precision ranging from 2.6 to 5.9% and 4.1–7.5% respectively. Analysis by HPLC-MS/MS was done with an Agilent XDB-C18 column (150 \times 2.1 mm ID, particle size 3.5 μm), a gradient mobile phase of 0.1% formic acid in water and 0.1% formic acid in methanol (0.4 mL/min) with MS/MS detection by dynamic MRM mode [26].

Similarly, by grafting an amphiphilic block copolymer consisting of poly(N-acryloyl-glucosamine) and poly(tert-butyl methacrylate) on magnetic MWCNTs (PAG/PGM-MNPs@MWCNTs) and using as a QuEChERS purification adsorbent coupled with HPLC-MS/MS, a total of 15 MYTs and 25 pesticides were detected in different grains (maize, wheat, rice and soy bean) [25]. Following a QuEChERS sample pretreatment method with 20 mL of 5% formic acid in acetonitrile as extraction solvent, 1.8 g NaCl+1g MgSO_4 +1g trisodium citrate+0.5 g disodium citrate as extraction powder and 50 mg of PAG/PGM-MNPs@MWCNTs as purification powder, the LOD, recovery and RSD of intraday plus interday precision ranging from 0.0011 to 1.3 ng/g, 60.8–108% and 1.9–16% respectively were reported for HPLC-MS/MS analysis of 15 MYTs in grain samples by using a XDB-C18 column (150 \times 2.1 mm ID, particle size 3.5 μm), a gradient mobile phase of 0.1% formic acid in water containing 5 mM ammonium formate and methanol (0.4 mL/min) and MS/MS detection in MRM mode. Compared to several commercially available QuEChERS adsorbents, the PAG/PGM-MNPs@MWCNTs was shown to exhibit higher adsorption capacity of interfering substances in matrix and substantially reduce matrix effects. In

Table 2. Carbon nanomaterials developed recently as solid phase extraction adsorbents for MYT analysis by liquid chromatographic methods.

MYTs	CNMs	Method	Chromatographic conditions and detection	Linear range	LOD, LOQ	Method Precision RSD; Application (Recovery)	Reference
ZEA, T-2 toxin, HT-2 toxin, neosolaniol, diacetoxyscirpenol	MNPs@MWCNTs (20 mg packed in SPE cartridge)	MSPE-UHPLC-MS/MS	Poroshell EC-C18 column (100 × 3 mm, 2.7 µm; mobile phase, H ₂ O & MeOH (1 mL/min); MS/MS (ESI)-MRM	0.1–500 ng/g (Std) 2–500 ng/g (Danshen)	0.45–1.80 ng/g, 1.20–4.80 ng/g	2.1–13.3%; Danshen- <i>Salviae miltiorrhizae</i> Radix et Rhizhoma (73.7–91.9%)	[29]
9 MYTs	rGO@AuNPs (10 mg packed in SPE cartridge)	MSPE-UHPLC-MS/MS	Poroshell EC-C18 column (100 × 3 mm, 2.7 µm); mobile phase, 5 mM NH ₄ CH ₃ CO ₂ in H ₂ O & MeOH (0.3 mL/min); MS/MS (ESI)-MRM	0.02–200 ng/mL	0.01–0.07 ng/mL, 0.02–0.18 ng/mL	2–14.9%; milk (70.2–111.2%)	[24]
20 MYTs	MNPs@MWCNTs (20 mg as QuEChERS purification powder)	QuEChERS-HPLC-MS/MS	Acquity Cortecs C18 column (100 × 2.1 mm, 1.6 µm); mobile phase, 5 mM NH ₄ CH ₃ CO ₂ in H ₂ O & MeOH (0.3 mL/min); MS/MS (ESI)-MRM	0.1–500 ng/g	0.002–5.446 ng/g	1.2–12.8%; grains-rice, millet, wheat, corn and coix seed (71.6–113.1%)	[10]
6 MYTs (6 aflatoxins)	Immunoaffinity rGO film@PBA/SA/mAB (30 mm in diameter)	IA-UPLC-MS/MS	Waters Acquity HSS C18 column (100 × 2.1 mm, 1.7 µm); mobile phase, ACN/MeOH (50:50, v/v) & 0.1% FA in H ₂ O (0.3 mL/min); MS/MS (ESI)-MRM	0.5–20 ng/mL	0.05–0.17 ng/mL, 0.16–0.50 ng/mL	2.5–9.4%; rabbit serum (55.1–75.3%)	[32]
15 MYTs	PAG/PGM-MNPs@MWCNTs (50 mg as QuEChERS purification powder)	QuEChERS-HPLC-MS/MS	Agilent XDB-C18 column (150 × 2.1 mm, 3.5 µm); mobile phase, 0.1% FA in H ₂ O+5 mM NH ₄ HCO ₂ & MeOH (0.4 mL/min); MS/MS-MRM	0.01–1000 ng/g	0.0011–1.3 ng/g	1.9–16%; grains-maize, wheat, rice and soy bean (60.8–108%)	[25]

12 MYTs	rGO@ZnONPs (15 mg for dSPE)	dSPE-UHPLC-MS/ MS	Poroshell EC-C18 column (100 × 3 mm, 2.7 µm); mobile phase, 5 mM NH ₄ CH ₃ CO ₂ in H ₂ O & MeOH (0.3 mL/ min); MS/MS (ESI)- MRM	0.1–200 ng/g	0.03–0.14 ng/g, 0.09 –0.41 ng/g	1.4–15%; Huanglian <i>Coptidis rhizome</i> (70.3 –105.7%)	[30]
13 MYTs	PEG- MNPs@MWCNTs (10 mg for dSPE)	MSPE-UHPLC- HRMS	Accucore aQ column (150 × 2.1 mm, 2.6 µm); mobile phase, 0.1% FA in H ₂ O & ACN (0.3 mL/ min); HRMS (± ioni- zation)-full scan mode	0.15–100 ng/mL	0.005–0.050 ng/mL, 0.015–0.150 ng/mL	2.1–11.7%; milk (81.8 –106.4%)	[28]
10 MYTs	PEI-GPMS- MNPs@MWCNTs (20 mg for dSPE)	MSPE-HPLC-MS/ MS	Agilent XDB-C28 column (150 × 2.1 mm, 3.5 µm); mobile phase, 0.1% FA in H ₂ O & 0.1% FA in MeOH (0.4 mL/min); MS/MS-MRM	0.02–200 ng/mL	0.003–0.442 ng/mL, 0.008–1.219 ng/mL	2.6–7.5%; milk (88.3 –103.5%)	[26]

MYTs, mycotoxins; ZEA, zearalenone; Std, standard; SPE, solid phase extraction; dSPE, dispersive solid phase extraction; MSPE, magnetic solid phase extraction; QuEChERS, quick, easy, cheap, effective, rugged and safe; MNPs@MWCNTs, Fe₃O₄ magnetic nanoparticles-multiwalled carbon nanotubes composite; PEG, polyethylene glycol; PEI, polyethyleneimine; GPMS, 3-glycidoxypentyltrimethoxysilane; PAG, poly(N-acryloyl-glucosamine; PGM, poly(tert-butyl methacrylate); rGO@AuNPs, reduced graphene oxide-gold nanoparticles composite; rGO@ZnONPs, reduced graphene oxide-zinc oxide nanoparticles composite; rGO film@PBA/SA/mAB, pyrenylbutyric acid, streptavidin and biotinylated monoclonal antibody conjugated to reduced graphene oxide film; IA, immunoaffinity; HPLC, high-performance liquid chromatography; UPLC, ultra-performance liquid chromatography; UHPLC, ultra-high-performance liquid chromatography; MS/MS, tandem mass spectrometric detection; ESI, electrospray ionization; MRM, multiple reaction monitoring; ACN, acetonitrile, MeOH, methanol; FA, formic acid; NH₄HCO₂, ammonium formate; NH₄CH₃CO₂, ammonium acetate; v/v, volume/volume; HRMS, high resolution mass spectrometry; LOD, limit of detection; LOQ, limit of quantitation; RSD, relative standard deviation.

another study, the application of 20 mg of magnetic MWCNTs ($\text{Fe}_3\text{O}_4/\text{MWCNTs}$) prepared without polymer was demonstrated as an efficient QuEChERS purification adsorbent for UPLC-MS/MS determination of 20 MYTs in different grains including rice millet, wheat, corn and coix seed [10]. A high sensitivity (LOD, 0.0021–5.4457 ng/g) with an acceptable recovery (71.6–113.1%) and high precision (intraday RSD, 1.2–12.7%; interday RSD, 1.5–12.8%) was reported for the same QuEChERS extraction powder as shown above with 25 mL of 1% acetic acid in acetonitrile/water (80:20, v/v) as extraction solvent for subsequent UPLC-MS/MS analysis using an Acquity Cortecs C18 column (100 × 2.1 mm ID, particle size 1.6 μm) with a gradient mobile phase of 5 mM ammonium acetate in water and methanol (0.3 mL/min) and MS/MS detection with electrospray ionization in MRM mode.

2.2. Graphene oxide-based SPE adsorbents

Similar to MWCNTs, graphene-based CNMs has gained attention recently for determination of food and environmental toxins [31]. However, their analytical application is limited due to its irreversible aggregation in solution caused by van der Waals force and π - π stacking interactions resulting in poor reliability, repeatability and specificity [30]. To remedy this problem, graphene-based CNMs are subjected to controlled oxidation to obtain rGO, followed by incorporation of another material such as metal nanoparticles to enhance the graphene interlayer distance for minimizing aggregation or conjugation with pyrenyl-based compounds for carboxylic acid enrichment enabling immobilization of antibodies [30,32]. Table 2 summarizes the various GO-based CNMs developed recently as SPE adsorbents for MYT analysis by liquid chromatographic methods. For example, Jiang et al. [24] developed a cartridge-based SPE with a nanocomposite of rGO and AuNPs by optimizing extraction solvent (5 mL of 1% formic acid in acetonitrile), rGO@AuNPs amount (10 mg), loading solvent (2% acetonitrile in water), washing solvent (5% methanol in water) and elution solvent (methanol/acetonitrile/formic acid, 50/49/1, v/v/v) for subsequent analysis of 9 MYTs including AFB1, AFM1, OTA, ZEA, zearalenone, α -zearalenol, β -zearalenol, α -zearalanol and β -zearalanol in milk by UHPLC-MS/MS. With a Poroshell EC-C18 column (100 × 3 mm ID, particle size 2.7 μm) and a mobile phase of 5 mM ammonium acetate in water (A) and methanol (B), all the 9 MYTs were separated within 9 min with

flow rate at 0.3 mL/min and column temperature at 40 °C. Based on quantitation by MRM mode, a good linear response was shown for the MYTs concentrations ranging from 0.02 to 200 ng/mL in milk samples, with the LOD at 0.01–0.07 ng/mL, LOQ at 0.02–0.18 ng/mL, recovery at 70.2–111.2% and precision RSD at 2–14.9%. In a later study, by employing a nanocomposite of rGO and ZnONPs, the same research group reported an improved dSPE-UHPLC-MS/MS method for analysis of 12 MYTs in a medicinal herb *Coptidis rhizoma* (Huanglian) widely used in Asian and European countries [30]. Using the same extraction and loading solvents as shown above [24], the remaining dSPE conditions such as rGO/ZnONPs amount (15 mg), washing solvent (n-hexane) and elution solvent (methanol/formic acid, 99/1, v/v) were optimized and the subsequent analysis by the same UHPLC-MS/MS method showed a linear response ranging from 0.1 to 200 ng/mL for 12 MYTs including AFB1, AFB2, AFG1, AFG2, AFM1, OTA, alternanol methyl ether, mycophenolic acid, penitrem A, nivalenol, zearalenone and zearalanone in *C. rhizoma* samples. Moreover, the validation parameters including LOD, LOQ, recovery and precision RSD were shown to be 0.03–0.14 ng/g, 0.09–0.41 ng/g, 70.3–105.7% and 1.4–15%, respectively [30].

In another study, Xie et al. [32] prepared immunoaffinity rGO films by conjugating with pyrenylbutyric acid, streptavidin and biotinylated monoclonal antibody (rGO@PBA/SA/mAB) for efficient adsorption of AFs including AFB1, AFB2, AFG1, AFG2, AFM1 and AFM2 for subsequent UPLC-MS/MS analysis. After optimization of adsorption time (30 min), desorption solvent (methanol), desorption solvent volume (5 mL) and desorption time (2 min), all the 6 AFs were separated within 5 min by using a Waters Acquity HSS T3 C18 column (100 × 2.1 mm ID, particle size 1.7 μm) and a mobile phase of acetonitrile/methanol (50:50, v/v) (A) and 0.1% formic acid in water (B) with flow rate at 0.3 mL/min and column temperature 40 °C. By using MRM mode, a linear response ranging from 0.5 to 20 ng/mL was shown with the LOD, LOQ and recovery respectively ranging from 0.05 to 0.17 ng/mL, 0.16–0.50 ng/mL and 55.1–75.3% in rabbit-serum samples, demonstrating that the antibody-functionalized rGO films possessed high adsorption efficiency for selective binding of AFs from an extremely low sample volume (100 μL). However, this technique requires a large volume of desorption solvent for complete immersion of film, which needs to overcome in the future design of such immunoaffinity films.

3. Electrochemical immunosensors based on carbon nanomaterials

Electrochemical immunosensors are based on immobilizing antibody with surface modified electrodes for highly sensitive analysis by selective binding through antibody–antigen interaction [33]. Given the high specific surface area and easy surface modification, the CNMs are deposited on electrodes, followed by functionalization with carboxylic acid, polymer or metal nanoparticles for immobilization of suitable target antibody [34]. The antibodies are immobilized by several techniques including covalent binding, self-assembly and electrostatic deposition, in which the covalent binding technique is often used due to the uniform immobilization of antibody attained through the amide bond formation between carboxylic acid groups on CNMs and amine groups on antibodies [22]. Prior to antibody immobilization, the carboxy-functionalized CNMs are usually activated using 1-ethyl-3-(3-dimethylaminopropyl)carbodiimide/N-hydroxy succinimide (EDC/NHS) coupling/activating agent for effective binding of antibody on the electrode surface [35–38]. Different electrodes employed include glassy carbon electrode (GCE), carbon screen printed electrode (CSPE), carbon electrode (CE), indium tin oxide electrode (ITO), dispense printed electrode (DPE) and GO-based microelectrode, while differential pulse voltammetry (DPV), cyclic voltammetry (CV), amperometry (AMP), electrochemical impedance spectroscopy (EIS), alternating current voltammetry (ACV) and linear sweep voltammetry (LSV) are among the electrochemical detection systems frequently used [23]. Various electrochemical immunosensors developed recently using CNTs, GO/rGO, and graphene quantum dots (GQDs) for detection of AFB1, ZEA, AFM1, OTA and PAT are discussed below and summarized in Table 3.

3.1. Carbon nanotube-based electrochemical immunosensors

The MWCNTs have emerged as a promising carbon nanomaterial especially in the fabrication of biosensors [3,22]. Specifically, the carboxylic acid-functionalized MWCNTs (cMWCNTs) are extensively used as they enable rapid and direct electron transfer in electrochemically active materials [39–41]. However, the aggregation problem in aqueous medium limits their application. To overcome this issue the fabrication of nanocomposites of cMWCNTs with a polymer such as chitosan (CH) and PEI or amino acid cysteine (CY) was shown to

effectively enhance the water-solubility, film-forming tendency and electrochemical signals for highly sensitive detection of AFB1 [36,42] and PAT [43]. For instance, Xu et al. [39] prepared a nanocomposite of cMWCNTs and chitosan (cMWCNTs/CH) to enhance the electrochemical signal for detection of ZEA at a low working voltage of 0.3 V. This immunoassay is based on an indirect competition between free ZEA and ZEA-bovine serum albumin (BSA) covalently conjugated to cMWCNTs/CH on GCE during immobilization of ZEA antibody. A LOD value of 4.7 pg/mL in a broader linear range (0.01–1000 ng/mL) was shown with high selectivity in the presence of DON, OTA, FB1 and AFB1, while a high recovery (94.0–106.4%) and high reproducibility (RSD, 1.88–2.43%) was attained. Also, the relative error values between this immunosensor assay and HPLC method was small, as evident by a range from 0.72 to 6.06% for corn, 0.25–1.26% for wheat and 0.25–1.26% for fodder, demonstrating a successful application to real food samples. For analysis of ZEA in the linear range of 0.005–50 ng/mL, Liu et al. [44] developed an amperometric immunosensor by modifying GCE with PEI-functionalized cMWCNTs, followed by electrodeposition of gold and platinum nanoparticles, immobilizing *Staphylococcus* protein A-based monoclonal antibody against ZEA (0.1 µg/mL for 60 min) and blocking with BSA (1% for 60 min). Under the optimum pH (7.4), incubation time (20 min) and working voltage (0.18 V), a sensitive voltammetric determination of ZEA was shown with a LOD at 1.5 pg/mL. Also, a high stability with 89% signal retaining after a 10-day storage period at 4 °C, high reproducibility (RSD, 2.13%) and high selectivity in the presence of α -zearalenol, β -zearalenol, zearalanone, α -zearalanol and β -zearalanol was attained, and its application to corn flour and corn-based baby food samples showed a ZEA recovery ranging from 90.4 to 106.4% and 87.7–109.0%, respectively. An ultrasensitive immunosensing assay in a narrow linear range of 0.0001–0.1 ng/mL with LOD at 0.15 pg/mL was reported by Riberi et al. [45] for determination of ZEA in maize samples by modifying CSPE with PEI-MWCNTs and immobilizing with ZEA polyclonal antibody-bonded AuNPs. The immunosensing principle is based on a direct competition between ZEA in maize samples and ZEA-labelled horseradish peroxidase (HRP) with an amperometric potential at –0.3 V and the reduction current produced by the remaining HRP is proportional to the amount of ZEA. A high reproducibility (RSD, <20%) and a high recovery (100.4%) in maize sample was observed, which

Table 3. Carbon nanomaterials-based electrochemical immunosensors developed recently for MYT analysis in food.

Mycotoxin	Carbon nanomaterial	Electrochemical detection	Probe	Linear range	LOD	Method reproducibility RSD; Application (Recovery)	Reference
AFB1	cMWCNTs/CH	DPV, CV	cMWCNTs/CH coated on CSPE, activated with EDC/NHS, coated with AFB1-BSA and immobilized with AFB1 antibody	0.1–10000 pg/mL	0.1 pg/mL	6.40%; palm kernel cake/corn kernel/soybean (77.6–117.4%)	[35]
AFB1	cMWCNTs/CY	EIS, CV	CY and cMWCNTs sequentially coated on GE by EDC/NHS, immobilized with AFB1 antibody and blocked with BSA	0.1–20 pg/mL	0.79 pg/mL	<5.0%; corn flour (107.9%)	[42]
ZEA	PEI-MWCNTs@Au/Pd NPs	DPV, CV	PEI-MWCNTs coated on GCE, electro-deposited with Au/Pd NPs, immobilized with ZEA antibody plus <i>Staphylococcus</i> protein A and blocked with BSA	5–50000 pg/mL	1.5 pg/mL	<2.13%; corn flour (90.4–106.4%) corn-based baby food (87.7–109.0%)	[44]
ZEA	cMWCNTs/CH	DPV, EIS, CV	cMWCNTs/CH coated on GCE, integrated with ZEA-BSA by EDC/NHS and immobilized with ZEA antibody	0.01–1000 ng/mL	4.7 pg/mL	1.88–2.43%; corn (94.0–106.4%)	[39]
AFB1	cMWCNTs/CH	DPV, CV	cMWCNTs/CH coated on CSPE, activated with EDC/NHS, coated with AFB1-BSA and immobilized with AFB1 antibody	0.1–10000 pg/mL	0.3 pg/mL	4.78%; peanut (80–127%)	[36]
ZEA	PEI-MWCNTs@AuNPs	AMP, CV	PEI-MWCNTs coated on CSPE conjugated with AuNPs, immobilized with ZEA polyclonal antibody and blocked with BSA	0.1–100 pg/mL	0.15 pg/mL	<20.6%; maize (100.4%)	[45]
AFM1	SWCNTs	AMP, CV	SWCNTs coated on DPE, anchored with antibody IgG, blocked with PVA and immobilized with AFM1 antibody	0.01–1 ng/mL	0.02 ng/mL	Milk (LOD, 0.026 ng/mL)	[47]
AFB1	GQDs/AuNPs	CV, EIS	GQD/AuNPs coated on ITO, activated with EDC/NHS and immobilized with AFB1-antibody	0.1–3.0 ng/mL	0.008 ng/mL	2.65%; maize (linear range, 0.1–2.5 ng/mL)	[37]
OTA	rGO/MoS ₂ –AuPdAg	DPV, EIS, CV	rGO/MoS ₂ –AuPdAg coated on GCE, immobilized with OTA antibody and blocked with BSA	0.01–150 ng/mL	0.005 ng/mL	3.25%; coffee and corn (103.6–107.0%)	[49]
OTA	SWCNTs	AMP, CV	SWCNTs coated on SE, immobilized with OTA antibody and blocked with PVA.	0.01–1 ng/mL	0.13 ng/mL	Grape juice (linear range, 0.01–1 ng/mL)	[48]
AFB1	GQDs/MoS ₂	EIS, CV	MoS ₂ /GQDs on ITO, activated with EDC/NHS, immobilized with AFB1 antibody and blocked with BSA	0.1–3.0 ng/mL	0.09 ng/mL	1.18%; maize (80.2–98.3%)	[38]
HT-2	ER-GO	DPV, EIS	Electrochemically reduced GO micro-electrodes inkjet printed on PEN, activated with EDC/NHS, immobilized with HT-2 antibody and blocked with BSA	6.3–100 ng/mL	1.6 ng/mL	Standard solution (87.8–108.5%)	[50]

AFB1	cMWCNTs/CH	EIS, CV	cMWCNTs/CH coated on disposable CE, activated with EDC/NHS, coated with AFB1-BSA, immobilized with AFB1 antibody and blocked with BSA.	1–30 ng/mL	0.62 ng/mL	7.8%; maize (97–99%)	[40]
PAT	GO	EIS	GO on GCE, activated with EDC/NHS, immobilized with PAT antibody and blocked with BSA	1–10 ng/mL	9.8 pg/mL	Apple juice (86%)	[43]
AFB1, OTA, ZEA	CdS/MoS ₂ /rGO/CNTs	CV, photo-electrochemical	CdS/MoS ₂ /rGO/CNTs coated on GCE, immobilized with respective antibodies and blocked with BSA	1–1000 pg/mL	AFB1: 0.17 pg/mL; OTA: 0.59 pg/mL; ZEA: 0.60 pg/mL	Millet and maize (comparable quantitation with HPLC-MS/MS method)	[52]
AFB1	Au@PEI@CNFs	DPV, CV	Au@PEI@CNFs coated on GCE, immobilized with AFB1 antibody and blocked with BSA.	0.05–25 ng/mL	0.027 ng/mL	4.66%; wheat (85.9–111.6%)	[46]
PAT	GO/AuNPs	DPV, EIS, CV	GO/AuNPs coated on GCE, immobilized with BSA-IgG PAT antibody and blocked with ovalbumin	5–200 ng/mL	5 ng/mL	—	[51]
AFB1	BP-cMWCNTs	DPV, EIS, CV	BP-cMWCNTs coated on GCE, immobilized with AFB1 antibody and blocked with BSA.	0.31–1561 pg/mL	0.084 pg/mL	1.28%; pu'er tea/rice (90.4–99.6%)	[41]

AFB1, aflatoxin B1; AFM1, aflatoxin M1; OTA, ochratoxin A; ZEA, zearalenone; PAT, patulin; HT-2, hydrolyzed T-2 trichothecene mycotoxin; CV, cyclic voltammetry; DPV, differential pulse voltammetry; EIS, electrochemical impedance spectroscopy; AMP, amperometry; cMWCNTs/CH, nanocomposite of carboxy-functionalized multi-walled carbon nanotubes and chitosan; PEI-MWCNTs@Au/Pd NPs, gold and palladium nanoparticles electrodeposited on polyethyleneimine-functionalized multi-walled carbon nanotubes; PEI-MWCNTs@AuNPs, gold nanoparticles immobilized on polyethyleneimine-functionalized MWCNTs; cMWCNTs/CY, carboxy-functionalized multi-walled carbon nanotubes covalently conjugated to cysteine self-assembled layer; Au@PEI@CNFs, 3D carbon nanofibers conjugated with AuNPs through polyethyleneimine; BP-cMWCNTs, cMWCNTs-functionalized black phosphorene; SWCNTs, single-walled carbon nanotubes; ER-GO, electrochemically reduced graphene oxide; GQDs/AuNPs, nanocomposite of graphene quantum dots and gold nanoparticles; rGO/MoS₂-AuPdAg, reduced graphene oxide decorated with few-layered molybdenum disulfide nanoroses and gold/palladium/silver trimetallic nanoparticles; GQDs/MoS₂, graphene quantum dots decorated on molybdenum disulfide nanosheets; GO/AuNPs, nanocomposite of graphene oxide and gold nanoparticles; PEN, poly(ethylene 2,6-naphthalate); CdS/MoS₂/rGO/CNTs, nanocomposite of cadmium sulfide/molybdenum disulfide/reduced graphene oxide/carbon nanotubes; GE, gold electrode; SE, silver electrode; GCE, glassy carbon electrode; CSPE, carbon screen printed electrode; CE, carbon electrode; DPE, dispense printed electrode; ITO, indium tin oxide electrode; EDC/NHS, 1-ethyl-3-(3-dimethylaminopropyl)carbodiimide/N-hydroxy succinimide; PVA, polyvinyl alcohol; BSA, bovine serum albumin; IgG, immunoglobulin G; LOD, limit of detection; RSD, relative standard deviation.

correlate well with that obtained by a HPLC-FLD method (104.6%).

A label-free electrochemical biosensor was developed by Costa et al. [42], who immobilized AFB1 antibody on cMWCNTs-conjugated self-assembled cysteine layer (cMWCNTs/CY) coated on gold electrode for detection of AFB1 in picogram range in corn flour. The voltammetric response due to a change in electrical conductivity is proportional to the concentration of AFB1 with the LOD, linear range and reproducibility being 0.79 pg/mL, 0.1–20 pg/mL and <5% RSD, respectively. Furthermore, this immunosensor attained a high mean recovery of 107.9% and high selectivity in the presence of OTA when applied to corn flour samples spiked with very low levels of AFB1 (0.1–15 pg/g), demonstrating a high sensitivity of this immunosensor which can be applied to food samples for onsite detection of AFB1. By using an indirect competitive ELISA method and EDC/NHS activation of carboxyl groups on cMWCNTs/CH-modified CSPE, Azri et al. [35] reported a much lower LOD value of 0.1 pg/g in a broader linear range of 0.1–10,000 pg/mL as well as a high repeatability (RSD, 7.6%), reproducibility (RSD, 6.4%) and recovery (77.6–117.4%) for AFB1 detection in samples of palm kernel cake, corn kernel and soybean, which can be attributed to the elevation of electrochemical surface area from 0.396 to 1.298 cm² enabling enhanced signal response of AFB1 following modification of the CSPE with cMWCNTs/CH. In a later study, following a similar fabrication approach of cMWCNTs/CH-modified CSPE, the same research group reported a LOD value of 0.3 pg/mL for the same linear range (0.1–10000 pg/mL) with a much lower RSD value for repeatability (4.8%) and reproducibility (2.7%), as well as high recovery (80–127%) when applied to peanut samples [36]. Principally, the above two studies [35,36] are based on an indirect competitive reaction between AFB1-BSA and free AFB1 for the binding site of a fixed amount of anti-AFB1 antibody. Upon treatment with the secondary antibody, a catalytic signal based on HRP generated in the presence of H₂O₂ and 3,3',5,5'-tetramethylbenzidine dihydrochloride (TMB) mediator results in a reduction peak for quantitation by DPV analysis. The fabrication of MWCNTs/CH with EDC/NHS activation was also adopted by Migliorini et al. [40], who developed a waterproof paper-based electrochemical immunosensor for AFB1 detection by drop-casting anti-AFB1 immobilized MWCNTs/CH film on a paper layered with graphite-based conductive ink. A LOD value of 0.62 ng/mL was shown in the linear range of 1–30 ng/mL with a high selectivity in a AFB1/OTA-

spiked sample as well as high intra- and inter-electrode reproducibility (RSD, 3.6% and 7.8%). Application to maize sample revealed a high recovery (97–99%) and the fabricated paper sensor was stable as evident by retaining 90% signal response over a 3-week storage period at 4 °C.

A comparative study between three-dimensional (3D) carbon nanofibers (CNFs) and CNTs coupled separately with AuNPs through PEI (Au@PEI@CNFs and Au@PEI@CNTs) was carried out by Huang et al. [46] for evaluation of their efficiency in the analysis of AFB1 in wheat samples. Following immobilization with AFB1 antibody, Au@PEI@CNFs showed a 3-fold lower LOD value (0.027 ng/mL) compared to Au@PEI@CNTs, with a linear DPV response ranging from 0.05 to 25 ng/mL. Also, a high reproducibility (RSD, 4.7%), high selectivity even with DON, OTA and ZEA and high stability with 90% signal response retained after one-week storage at 4 °C as well as a high recovery (85.9–111.6%) was shown, demonstrating a successful application of this Au@PEI@CNFs-based immunosensor to wheat samples. More specifically, a relatively higher sensitivity of Au@PEI@CNFs can be attributed to the unique hierarchically arranged 3D porous structure of bacterial cellulose-derived CNFs facilitating faster electrolyte diffusion and larger electrochemical surface area for enhanced peak current response by DPV analysis. More recently, an ultralow LOD value (0.084 pg/mL) was reported for an electrochemical immunosensor fabricated by immobilizing anti-AFB1 nanobody on black phosphorene-functionalized cMWCNTs coated on GCE [41]. This immunosensor was shown to be extremely sensitive in the linear range of 0.31–1561 pg/mL with a high reproducibility (RSD, 1.3%) and good selectivity even with AFB2, AFG1, AFG2, OTA, ZEA and DON as well as high stability with 85.6% signal response retained over a 13-day storage period at 4 °C. Also, a high recovery was obtained for its application to AFB1 analysis in pu'er tea (90.4–99.6%) and rice (90.7–95.9%) samples. Additionally, this sensor showed good anti-fouling property without losing its efficiency in the presence of even 500-fold higher concentration of MgSO₄, KCl, FeCl₃, vitamin C, CaCl₂ and catechin.

While most studies deal with electrochemical sensors with rigid electrode, some recent studies have reported the use of flexible and stretchable/bendable sensors. To overcome the problems associated with mask usage and high ink consumption in screen printing technique, Abera et al. [47] used a mask-free dispense-printing method to fabricate flexible electrodes coated with SWCNTs and immobilized with immunoglobulin (IgG)

monoclonal antibody for electrochemical immunosensing detection of AFM1 in milk samples by chronoamperometry. A LOD value as low as 0.02 µg/L (buffer) and 0.026 µg/L (milk) was shown in the linear range of 0.01–1 µg/L. This flexible dispense-printing technique is promising in fabricating immunosensors in different shapes tailored for specific applications. In a later study, the same research group prepared stretchable and bendable OTA-selective biosensors by screen printing respectively on polydimethylsiloxane (PDMS) and polyethylene terephthalate [48]. After coating working electrodes with SWCNTs and immobilizing with OTA antibodies, they were shown to detect OTA selectively in grape juice in the presence of AFM1 with a LOD value at 0.13 ng/mL for the stretchable sensor and 0.08 ng/mL for the bendable sensor in the linear range of 0.01–1 ng/mL, which is lower than the maximum allowable limit set by EU (0.025 ng/g for infants and 0.05 ng/g for adult).

3.2. Graphene and graphene oxide-based electrochemical immunosensors

Besides CNT-based electrochemical immunosensors, some other GO/rGO and GQD-based electrochemical immunosensors are also developed for MYT analysis in food (Table 2). For example, Sharifuzzaman et al. [49] synthesized rGO/MoS₂ nanoroses by green method using sodium periodate and conjugated with trimetallic NPs (AuPdAg NPs) for label-free detection of OTA in coffee and corn samples, with rGO acting as branches carrying electrons instantly from electrode surface to MoS₂-NRs, while the L-proline-assisted Au/Pd/Ag NPs on active sites of MoS₂-NRs enabled direct immobilization of anti-OTA antibody for enhanced electrocatalytic activity by accelerating the electron transport at the electrode interface. The as-prepared rGO/MoS₂-NRs/AuPdAg NPs nanocomposite exhibited excellent electrochemical performance for detection of OTA in the linear range of 0.01–150 ng/mL with the LOD being 0.005 ng/mL. Also, the developed OTA immunosensor showed high stability upon storage up to 10 weeks without any significant change in current intensity and a high recovery ranging from 104.3 to 107.0% and 103.6–106.0% for OTA-spiked coffee and corn samples respectively confirmed its application potential to real food samples. In a later study, Kudr et al. [50] formulated a water-based GO ink and single-drop working electrode was inkjet-printed on poly(ethylene 2,6-naphthalate) substrate, followed by electrochemical reduction of GO and detection of HT-2 mycotoxin through carbodiimide linking of

microelectrode surface with HT-2 toxin antibody. This biosensor reported a linear response ranging from 6.3 to 100 ng/mL with LOD value at 1.6 ng/mL and recovery in standard solution ranging from 87.8 to 108.5%.

In two different studies by the same research group, GQDs conjugated with AuNPs or MoS₂ nanosheets were reported to enhance the electrochemical immunosensing performance for sensitive detection of AFB1 in maize samples [37,38]. In the former study, the GQDs-AuNPs nanocomposite fabricated through conjugation of carboxyl groups of GQDs and amino groups of the crosslinker 2-aminothiophenol was dispersed on an ITO electrode and subsequently immobilized with AFB1 antibody for AFB1 detection in maize samples [37]. A linear response was shown for the AFB1 concentrations ranging from 0.1 to 3.0 ng/mL with LOD at 0.008 ng/mL and a high precision (RSD, 2.65%) as well as high selectivity in the presence of OTA were demonstrated. This immunoelectrode also showed acceptable stability with 94% current signal retained after storage at 4 °C for 4 weeks. Comparatively, the latter study demonstrated a more pronounced electrochemical response of GQDs upon conjugating with CTAB-exfoliated MoS₂ nanosheets for detection of AFB1 in maize samples [38]. After electrophoretic deposition of MoS₂@GQDs on ITO electrode and immobilization with AFB1 antibody by EDC/NHS crosslinker, a linear signal response in the same AFB1 concentration range (0.1–3.0 ng/mL) with LOD at 0.09 ng/mL was shown, while a high recovery ranging from 80.2 to 98.3% was reached from the AFB1-spiked maize samples [38]. The electrochemical parameters such as diffusion coefficient (1.67×10^{-5} cm²/s) and heterogeneous electron transfer (2×10^{-5} cm/s) for the fabricated AFB1 antibody/MoS₂@GQDs/ITO immunosensing electrode revealed excellent performance due to abundantly exposed edge sites, large surface area, improved electrical conductivity and electrocatalytic activity.

Electrochemical immunosensors involving deposition of GO or GO/Au nanocomposite on GCE are also studied for determination of PAT in apple juice. Riberi et al. [43] developed a label-free electrochemical immunosensor by depositing GO on GCE, followed by immobilizing polyclonal anti-PAT antibody with oxygen groups of GO and analyzing by EIS. The current response showed a linearity in the PAT concentration ranging from 1×10^{-2} –10 ng/mL with a LOD value of 9.8 pg/mL and half-maximal inhibitory concentration (IC₅₀) of 360 pg/mL. Moreover, a PAT recovery of 86% from apple juice was shown, demonstrating a successful

application of determining PAT in beverages without requiring any sample pretreatment step. More recently, the GO/Au nanocomposite-coated GCE immobilized with rabbit anti-patulin-BSA IgG was fabricated by Song et al. [51] for determination of PAT in standard solution. In principle, the electron transfer in the developed rabbit anti-PAT-BSA IgG-GO/Au-GCE immunosensor is initially blocked by IgG-related spatial hindrance resulting in a high resistance. However, in the presence of PAT, the immobilized IgG interacts with PAT resulting in a decline in the resistance and a simultaneous increase in electric current enabling PAT detection in the linear range of 5–200 ng/mL. This immunosensor can detect PAT at levels as low as 5 ng/mL (LOD) within 1 min without any cross reactivity even with 1000 ng/mL of added OTA. However, a significant cross reactivity does occur with BSA, limiting its use in samples containing BSA.

3.3. Carbon nanotube and graphene oxide combo-based electrochemical immunosensor

For effective and simultaneous detection of multi-MYTs, a flexible 3D film composed of CdS NPs, MoS₂ nanoflakes, rGO and CNTs was synthesized and placed on an adhesive tape pasted on various substrates such as fluorine doped tin oxide (FTO), ITO and GCE, followed by decorating the 3D-film electrode with different antigens, incubating with a mixture of AFB₁, OTA and ZEA and measuring both photoelectrochemical and CV responses [52]. Compared to 3D-film on FTO and ITO, the removable/renewable tape-pasted film on GCE showed a lower LOD value of 0.17 pg/mL for AFB₁, 0.59 pg/mL for OTA and 0.60 pg/mL for ZEA in the linear range of 1–1000 pg/mL without any cross-reactivity when measured with only one antigen–antibody combination. Also, it exhibited high stability with 95% signal response maintained after storage of fabricated electrodes for 4 weeks. For analysis of AFB₁, OTA and ZEA in millet/maize by this method, the quantitative data were 3.8/6.0, 58.2/76.5 and 0/6.1 ng/g, respectively, which was comparable to that obtained by HPLC-MS/MS method (4.2/6.1, 60.1/82.0 and 0/6.2 ng/g), demonstrating the reliability and effectiveness of this immunosensing method for multimycotoxin analysis. Most importantly, this method with dual current response measurement by photoelectrochemical and CV possesses the advantage of overcoming both false-positive and false-negative signals.

4. Electrochemical aptasensors based on carbon nanomaterials

Aptamers are single stranded DNA or RNA with small fragments of oligonucleotide sequences containing 10 to 100 nucleotide bases [19]. They are usually selected from a combinatorial DNA library by systematic evolution of ligands exponential enrichment (SELEX) technology for binding to target analyte through folding into specific 3D-structures [34,53]. Aptamers possess a remarkable ability to interact with a wide range of molecular targets with high selectivity [54]. Unlike antibodies, aptamers are of low cost and easy to prepare with reproducible synthesis and exhibit high chemical and thermal stability with no significant toxicity [55]. Most importantly, electrochemical sensors with aptamer as recognition element produce rapid response with high sensitivity and require only a small sample amount. Table 4 summarizes various CNMs-based electrochemical aptasensors developed recently for analysis of MYTs in food.

4.1. Carbon nanotube-based electrochemical aptasensor

An amperometric aptasensor was developed for OTA analysis by using a modified screen-printed gold electrode (SPGE) containing OTA aptamer as sensing ligand, methylene blue as redox indicator, SWCNTs as signal amplifiers and aptamer complementary strands (CSs) as assisting DNA [56]. The analytical principle is based on weakening of electrochemical signal caused by release of methylene blue and SWCNTs due to detachment of aptamer/CSs duplex in the presence of OTA. A high reproducibility (RSD, 6.3%) was shown with high selectivity in the presence of AFB₁, AFG₁, DON, ZEA, ricin A, acetamiprid and warfarin. Also, a linear response ranging from 72.7 to 12114 pg/mL as well as a LOD of 21.0, 23.4 and 54.1 pg/mL for water, grape juice and serum samples were reported, respectively [56].

4.2. Graphene-based electrochemical aptasensor

4.2.1. Atom-doped graphene aptasensor

Doped graphene sensor platforms have gained attention recently due to their improved electrochemical performance, which depends on various factors such as doping condition, precursor type, molecular structure of analyzed probe, structural defect, amount of oxygen functionality and surface area [57]. Moreover, several reports have shown that the structural features exhibit greater influence on

Table 4. Carbon nanomaterials-based electrochemical aptasensors developed recently for MYT analysis in food.

Mycotoxin	Carbon nanomaterial	Electrochemical detection	Aptamer	Linear range	LOD	Method reproducibility RSD; Application (LOD/Recovery)	Reference
OTA	SWCNTs	DPV, CV	OTA aptamer: 5'-GATCGGGTGTGGGTGGCGTAA AGGGAGCATCGGACA-3', CS1: 5'-Thiol-CAACATTT GTCCGATGCTCC-3', CS2: 5'-CCACCCACACCCGATC TTACCAAACCACC GCCTCCA-NH ₂ -3' (FAM labeled)	72.7–12114 pg/mL	21 pg/mL	6.3%; grape juice (23.4 pg/mL); Serum (54.1 pg/mL)	[56]
FB1	B/N ₂ -doped GR	EIS, CV	5'-CGATCTGGATATTATTTTGATACCCCTTT GGGGAGACAT-3' (FAM labeled)	0.0007–18.1 pg/mL	12.3 pg/mL	–	[59]
ZEA	N ₂ -doped GQDs on NH ₂ -Ru@SiO ₂ NPs	ECL, CV	5'-GGAATTCCTGTGATGTTGCCTGGGATTGTTTG GGCCTTGTGTTTTCTCCGTTCCAACCTAGTAG GATCCCGAA-NH ₂ -3' (5'-GATCGGGTGTGGGTGGCGTAAA GGGAGCATCGGACA-3')-5'-SH	0.01–10000 pg/mL	0.001 pg/mL	1.89%; corn flour (92.1–111.1%)	[60]
OTA	PEDOT-AuNFs@3D-GO sponge	DPV, CV	(5'-GATCGGGTGTGGGTGGCGTAAA GGGAGCATCGGACA-3')-5'-SH	10–20000 ng/mL	4.9 ng/mL	4.3%; wine (97.2–106.7%)	[63]
AFB1	AuNPs@thionine-rGO	ACV, EIS	cDNA: 5'-CGAGACACAGAGAGACAACACGTGCC CAAC-(CH ₂) ₆ -SH-3' 5'-GTTGGGCACGTGTTGCTCTCTGTGTCTCGTGCC CTTTCGCTAGGCCACACA-3' (ferrocene labeled)	0.05–20 ng/mL	0.016 ng/mL	1.79%; peanut (86.5–112.0%)	[66]
AFB1	LbL PDDAC-GR/cPS	EIS, CV	5'-NH ₂ -TGGGGTTTTGGTGCGGGTGGTGTAC GGGCGAGGG-3' 5'-NH ₂ -C6-GCATCACTACAGTCATTACGCATCGTAG GGGGGATCGTTAAGGAAGTGCCCGGAGGCGG TATCGTGTGAAGTGCTGTCCC-3'	0.001–0.10 ng/mL	0.002 ng/mL	1.4%; oil (94.5%); soy sauce (103.3%)	[64]
DON	3D GR-Ni/iron oxide NFs	Voltammetry (picoammeter)	5'-NH ₂ -C6-TCATCTATCTATGGTACATTA CTATCTGTAATGTGATATG-3'	0.001–1000 pg/mL	2.11 pg/mL	Rice (<i>Oryza sativa</i>) (NCR)	[62]
ZEA	CH@AB-MWCNTs	DPV, CV	5'-TCATCTATCTATGGTACATTACTATCTGTAATG TGATATG-(CH ₂) ₆ -NH ₂ -3' 5'-TAATGTACCATAGATAGA TGA-(CH ₂) ₆ -NH ₂ -3'	1 × 10 ¹ -1x10 ⁶ fg/mL	3.64 fg/mL	7.7%; corn oil and corn flour (92.8–111.5%)	[67]
ZEA	3D GR-Ni/iron oxide NFs	EIS	5'-NH ₂ -C6-TCATCTATCTATGGTACATTA CTATCTGTAATGTGATATG-3'	0.001–1000 pg/mL	0.001 pg/mL	–	[61]
OTA	GR-FET	FET	5'-GATCGGGTGTGGGTGGCGTAAAGGGAGCAT CCGACA-3'	2–202 pg/mL	0.57 pg/mL (PBS)	NCR; red wine (0.4 pg/mL); white wine (1.2 pg/mL)	[65]

OTA, ochratoxin A; FB1, fumonisin B1; ZEA, zearalenone; DON, Deoxynivalenol; AFB1, aflatoxin B1; SWCNTs, single-walled carbon nanotubes; B/N₂-doped GR, boron- or nitrogen-doped graphene; N₂-doped GQDs on NH₂-Ru@SiO₂ NPs, electrostatically coupled tris (2,2-bipyridyl)ruthenium-doped silica nanoparticles with nitrogen-doped graphene quantum dots; 3D GR-Ni/iron oxide NFs, three-dimensional graphene-nickel decorated with rose petal-shaped iron oxide nanoflowers; PEDOT-AuNFs@3D-GO sponge, poly (3,4-ethylenedioxy thiophene)-gold nanoflowers composite (PEDOTAuNFs) supported on three-dimensional graphene oxide sponge; GR-FET, graphene-based field effect transistor; AuNPs@thionine-rGO, thionine-functionalized reduced graphene oxide mixed with gold nanoparticles; LbL PDDAC-GR/cPS, layer-by-layer alternate deposition of positively-charged poly(diallyldimethylammonium chloride) modified graphene nanosheets and negatively-charged polystyrene nanospheres; 3D GR-Ni/iron oxide NFs, iron oxide nanoflowers electrochemically deposited on 3D graphene-nickel substrate; CH@AB-MWCNTs, chitosan functionalized acetylene black and multi-walled carbon nanotubes nanocomposite; CV, cyclic voltammetry; ACV, alternating current voltammetry; DPV, differential pulse voltammetry; EIS, electrochemical impedance spectroscopy; ECL, electrochemiluminescence; FET, field effect transistor; CS1, complementary strand 1; CS2, complementary strand 2; FAM, fluorescein amidite or carboxyfluorescein; LOD, limit of detection; RSD, relative standard deviation; NCR, high reproducibility with no significant change in detector response; PBS, phosphate buffered saline.

electrochemical behavior than the amount and type of dopant [58]. In line with this hypothesis, Tian et al. [59] compared the efficiency of boron-doped, nitrogen-doped and undoped graphene for detection of FB1 and reported that the oxygen functionality on doped graphene instead of the type/amount of dopant had a strong influence on the sensitivity of impedimetric signal. The boron-doped graphene (electron donating n-type) substrate with least oxygen functionality showed the highest electrochemical response, followed by nitrogen-doped graphene (electron accepting p-type) and undoped graphene substrates. In other words, the lower the concentration of oxygen functionality on graphene surface, the higher the immobilization of FB1-aptamer by physical adsorption and more sensitive detection of FB1. Thus, by using the highly efficient boron-doped graphene, a LOD value of 12.3 pg/mL in the linear range of 0.0007–18.1 pg/mL with good selectivity for FB1 in the presence of OTA was shown [59].

In a later study, a self-assembled luminophore by electrostatically immobilizing nitrogen-doped GQDs on amine-functionalized Tris (2,2-bipyridyl) dichlororuthenium (II) hexahydrate-doped silica nanoparticles ($\text{NH}_2\text{-Ru@SiO}_2$ NPs) for electrochemiluminescence (ECL) detection of ZEA in corn flour [60]. The optimized aptamer concentration (1 μM), reaction time between nitrogen-doped GQDs and $\text{NH}_2\text{-Ru@SiO}_2$ NPs (10 h), binding time of ZEA with aptamer (60 min) and buffer pH (7.0) showed excellent ECL detection of ZEA due to short electron-transfer distance and minimum energy loss with a LOD of 0.001 pg/mL in the linear range of 0.01–10000 pg/mL. In addition, a high reproducibility (RSD, 1.89%) and storage stability (96.2% response signal retained after two-week storage at 4 °C) was reported with high selectivity in the presence of AFB1, OTA, FB1 and their mixtures. Application to corn flour samples revealed a mean recovery of 100.2% by this ECL sensor, which are in accordance with that obtained by UPLC-MS method (111.1%). Also, this ECL sensor showed a much lower LOD (0.09 ng/mL) of ZEA than that by UPLC-MS (90 ng/mL). Likewise, an ultralow LOD (0.001 pg/mL) was reported for ZEA detection in the linear range of 0.001–1000 pg/mL by using 3D graphene-nickel decorated iron nanoflowers (transducer) and ZEA aptamer (bioreceptor) [61]. Such high sensitivity of ZEA detection can be due to the unique nanostructure with large surface area for immobilization, high electrical conductivity and enhanced charge transfer on nanomaterial surface. Moreover, this impedimetric biosensor is highly selective towards ZEA detection in the presence of

DON and OTA. Similarly, a sensor prepared by electrochemical deposition of 3D graphene-nickel on iron nanoflowers could detect DON at a LOD of 2.11 pg/mL with a linearity ranging from 0.001 to 1000 pg/mL as well as a high reproducibility (RSD, 4.09%) and high selectivity in the presence of ZEA and OTA [62].

4.2.2. Conducting polymer-functionalized graphene aptasensors

Conducting polymers with high stability are successfully used in electrochemical signal enhancement. An electrochemical aptasensor consisting of poly(3,4-ethylenedioxy thiophene)-gold nanoflowers composite (PEDOT-AuNFs) supported on 3D-graphene oxide sponge (GOS) was shown to provide ultrasensitive detection of OTA by multiple signal amplification by GOS and PEDOT-AuNFs [63]. PEDOT, an excellent conducting polymer with high stability, was conjugated with AuNFs using an ionic-liquid (1-methyl-3-octyl-imidazolium chloride)-assisted technique and the unique hierarchical flower-like structure provided high surface area for enhanced electron transfer and increased active sites for immobilization of aptamer through Au-S interaction. A LOD value of 4.9 ng/mL with a linear range of 10–20000 ng/mL, a high specificity in the presence of tartaric acid, lactic acid and malic acid, and high reproducibility (RSD, 4.3%) was obtained, along with a good storage stability at 4 °C with 95% signal retained after 2 weeks. Also, the application to wine samples showed a high recovery ranging from 97.2 to 106.7%, demonstrating that this aptasensor can be a promising biosensor for OTA detection in food commodities. In a later study, an electrochemical aptasensor was developed through layer-by-layer self-assembly of positively charged poly(diallyldimethylammonium chloride)-graphene nanosheets and negatively charged carboxylated polystyrene nanospheres on the electrode [64]. After immobilization of AFB1 aptamer on the surface of carboxyl-functionalized polystyrene nanospheres via an amide bond, the multi-layered sandwich-structured electrode exerted excellent conductivity and abundant electrochemically active sites for sensitive detection of AFB1 with LOD at 0.002 ng/mL in the linear range of 0.001–0.10 ng/mL with high reproducibility (RSD, 1.4%) and high recovery from oil (94.5%) and soy sauce (103.3%). In addition, this aptasensor showed long-term stability as evident by retaining 85% of signal intensity over a 30-day storage period at 4 °C.

More recently, Nekrasov et al. [65] designed an advanced biosensor for OTA detection by using an array of graphene-field-effect transistors (GFET)

integrated on a single silicon chip by adopting pyrenebutanoic acid/succinimide ester (PBASE) chemistry. An electric field stimulation promoted more efficient π - π stacking of PBASE to graphene as well as G-rich aptamer to graphene. In the presence of OTA, the aptamer changed its secondary configuration to G-quadruplex providing an accurate and rapid electrical response, with the liquid-gate configuration in terms of liquid properties such as pH and ionic strength affecting the GFET performance. Buffer with low ionic strength was shown to increase this sensor's sensitivity by 10-fold in the linear range of 2–202 pg/mL with the response time and LOD being 10 s and 0.57 pg/mL in phosphate buffered saline respectively as well as 50 s and 0.4–1.2 pg/mL in wine samples, accompanied by a high selectivity in the presence of AFM1 [65]. Consequently, this GFET-based electrochemical aptasensor is expected to detect multiple MYTs using a single chip following proper patterning and assembling of several MT-specific aptamers.

4.2.3. Other functionalized graphene aptasensors

A redox probe thionine with good electrochemical stability, reversibility and fast electron transfer properties was used to conjugate with rGO, followed by dispersing AuNPs on thionine-rGO for exerting high electrical conductivity and surface area as well as synergistic charge transfer [66]. In principle, the ferrocene-labelled aptamer in AuNPs@thionine-rGO forms a conjugate with AFB1, resulting in detachment from the electrode accompanied by a decrease in current intensity. This ratiometric aptasensor showed linearity in the AFB1 concentration ranging from 0.05 to 20 ng/mL with LOD at 0.016 ng/mL. A high reproducibility with RSD at 1.79% as well as high selectivity even with FB1, AFB2, ZEA and OTA and a negligible change over a 7-day storage period at 4 °C was shown. Application to peanut samples demonstrated a high recovery (86.5–112.0%) of AFB1 and the accuracy was comparable to that obtained by HPLC-FLD method (99.6–123%).

4.3. Carbon nanotube and graphene oxide combobased electrochemical aptasensor

A signal-on aptasensor based on target-induced amplification strategy was recently reported for highly sensitive detection of ZEA [67]. By using a nanocomposite composed of chitosan-functionalized acetylene black and MWCNTs (CH@AB-MWCNTs) for enhancement of surface area and conductivity as well as AuNPs and carboxylated

GO-labeled ZEA aptamer for signal enhancement, an ultralow LOD value of 3.64 fg/mL in a broader linear range of 1×10^1 – 1×10^6 fg/mL was attained for highly sensitive detection of ZEA. Moreover, this method possesses excellent selectivity even with aflatoxin mixture, OTA and β -zearalanol as well as high reproducibility (RSD, 7.7%) and good stability with 92% signal response retained after 15-day storage at 4 °C. In addition, a high recovery ranging from 92.8 to 99.6 and 101.2–111.5% was shown for corn oil and corn flour, respectively.

5. Fluorescence aptasensors based on carbon nanomaterials

Fluorescence-based biosensors involving GO, rGO, GOQDs, single-walled carbon nanohorns (SWCNHs) and cMWCNTs have been developed recently for analysis of MYTs. Various parameters characterized in fluorescence biosensors include fluorescence anisotropy, intensity, decay time, energy transfer, quenching efficiency and quantum yield. Different fluorescence formats, types of fluorescence labels, criteria for selection of a fluorescent label and various types of nanomaterials employed as fluorophores and quenchers are well documented by Sharma et al. [20] and Krishnan et al. [68]. In the following sections, various novel fluorescence-based aptasensors developed recently using CNMs for analysis of MYTs in food are discussed and summarized in Table 5.

5.1. Graphene-based fluorescence aptasensors

5.1.1. Graphene tubular micromotor-based fluorescence aptasensors

Given the high cost and complexity of conventional fabrication methods, the template electro-synthesis methods offer versatile approach in exploring micromotors with new structures and compositions for improved functionalization and catalytic performance. Especially, the chemically powered micromotors exhibit efficient self-propulsion property along with mixing effect for continuous movement around the sample enabling frequent contact with target for enhanced binding efficiency and detection sensitivity through micro-bubbles generation [69]. Owing to their large surface area and unique surface property, graphene materials are recently used to develop tubular micromotors capable of attaining high target accessibility and target capture [70]. In addition, they allow incorporation of different receptors for capturing a wide variety of targets and can be used for analysis of samples with low volume.

Table 5. Carbon nanomaterials-based fluorescence aptasensors developed recently for MYT analysis in food.

Mycotoxin	Carbon nanomaterial	Aptamer	Principle	Linear range	LOD, LOQ ^a	Method Precision RSD; Application (Recovery)	Reference
ZEA	Exfoliated carboxy-GO	5'-AGCAGCACAGAGGTCAGATGTCATCTATCTAT GGTACATTACTATCTGTAATGTGATATGCCTATGCG TGCTACCGTGAA-3'	ZEA turns-on the FL of FAM-labelled aptamer quenched by carboxy-GO.	0.5–64 ng/mL	0.5 ng/mL	2.4–3.6%; beer and wine (87–96%)	[77]
OTA, FB1	rGO/PtNPs micromotors	OTA: 5'-GGGAGGACGAAGCGGAACCGGGTGTGG GTGCCTTGATCCAGGGAGTCTCAGAAGACACGCC GACA-3' FB1: 5'-ATACCAGCTTATTCAATTAATCGCATTATA CCAGCTTATTCAATTACGTCTGCACATACCAGCTTA TTCAATTAGATAGTAAGTGCAATCT-3'	OTA & FB1 turn-on the FL of FAM-labelled aptamer quenched by rGO/PtNPs.	OTA: 1–1000 ng/mL FB1: 10–1000 ng/mL	OTA: 7, 10 ng/mL FB1: 0.4, 1 ng/mL	<9%; wine and beer (96–98%)	[69]
OTA	GO	APT: 5'-GATCGGGTGTGGGTGGCGTAAA GGGAGCATCGGACA-3' cAPT: 5'-CGCCACCCACACCCGATC-3'	OTA detaches cAPT from APT/cAPT and conjugates with RNA-labelled fluorophore to release fluorophore by hydrolysis.	0.08–200 ng/mL	0.08 ng/mL	Red wine (90.9–112.0%)	[79]
OTA, FB1	rGO/Ni/PtNPs micromotors	OTA: 5'-GGGAGGACGAAGCGGAACCGGGTGTGG GTGCCTTGATCCAGGGAGTCTCAGAAGACACGCC GACA-3' FB1: 5'-ATACCAGCTTATTCAATTAATCGCATTATA CCAGCTTATTCAATTACGTCTGCACATACCAGCTTA TTCAATTAGATAGTAAGTGCAATCT-3'	OTA & FB1 turn-on the FL of RhX-labelled aptamer quenched by rGO/PtNPs.	OTA: 5–1000 ng/mL FB1: 10–1000 ng/mL	OTA: 4 ng/mL FB1: 0.7 ng/mL	<7%; wine (104–108%)	[70]
OTA	CeO ₂ -GOQDs	OTA: 5'-GATCGGGTGTGGGTGGCGTAAAAGGGAG CATCGGACA-3'. DNA1: 3'-NH ₂ -(TTT) ₃ CTAGCCACACC-5' DNA2: 3'-CTC GTAGCCTGT(TTT) ₃ -NH ₂ -5'	OTA turns-on the FRET (DNA1@CeO ₂ and DNA2@GOQDs) quenched by aptamer.	10–20000 pg/mL	2.5 pg/mL	Peanut (90–110%)	[72]
OTA	SWCNHs	HP: 5'-TCCCTTTACGCCCTTTTGATCG GGTGTGGGTGGCGTAAAGGGAGCATCGGACA-3' SP: 5'-GGCGTAAAGGGA-3'	OTA turns-on the FL of SP quenched by SWCNHs through binding with aptamer in HP, exposing EXO III to digest SP and releasing free fluorophore	4.04–403.8 ng/mL	1.7 ng/mL	<6.3%; beer and Red wine (92.0–115.9%)	[84]
AFM1	GO	5'-TCCGTCACACCTGCTCTGACGCTGGG GTCGACCCG-3'	AFM1 turns-on the FL of FAM-labelled aptamer quenched by GO.	0.2–10 ng/g	0.05 ng/g	Infant milk powder (92–126%)	[80]
AFB1	GO	5'-GTTGGGCACGTGTTGTCTCTCTGTGT CTCGTGCCCTTCGCTAGGCCACACA-3' (FAM labelled)	AFB1 decreases the FL polarization of aptamer/GO by conjugating with the detached aptamer	0.016–1.56 ng/mL	0.016 ng/mL	2.4–3.6%; rice (89.2–112.0%)	[78]

AFB1, FB1	GO/Fe ₃ O ₄ nanocomposite	AFB1: 3'-NH ₂ -ACACCCGGATCGCTTCCCGTGCTTCC CGTGCTCTGTGTCTC TCTGTTGTGCACGGGTTG-5' FB1: 5'-ATACCAGCTTATTCAATTAATCGCATTACC TTATACCAGCTTATTCAATTACGTCTGCACATACCA GCTTATTCAATTAGATAGTAAGTGCAATCT-NH ₂ -3'	AFB1 and FB1 turn-on the FL of aptamer-labelled CdTe QDs quenched by GO/Fe ₃ O ₄ .	AFB1: 0.01–100 ng/mL FB1: 16.2 pg/mL	AFB1: <6.3%; peanut (92–97%) FB1: 6.7 pg/mL 16.2 pg/mL	[73]
AFB1, OTA	GO	AFB1: 5'-GTTGGGCACGTGTTGTCTCTCTGTGTCTC GTGCCCTTCGC-3' OTA: 5'-GATCGGGTGTGGGTGGCGTAAAGGG AGCATCGGACA-3'	AFB1 and OTA turn-on the FL of FAM-labelled AFB1 aptamer and Texas red-labelled OTA aptamer quenched by GO.	AFB1: 5–60 ng/mL OTA: 100–800 ng/mL	AFB1: 3.312 ng/mL OTA: 15.17 ng/mL	Wine (82.7–112.6%) [75]
PAT	cMWCNTs	5'-GGCCCCGCAACCCGCATCATCTACACTGATATT TTACCTT-3'	PAT turns-on the FAM-labelled aptamer quenched by cMWCNTs.	0.005–0.3 ng/mL	0.13, 0.41 µg/mL	<4%; apple juice (96–98%) [85]
ZEA, OTA	GO-based steganographic aptasensor	ZEA: 5'-CTACCAGCTTTGAGGCTCGATCCAGCTTA TTCAATTATACCAGCTTATTCAATTATACCAGC-3' (Cy3 labelled) OTA: 5'-AGCCTCGTCTGTTCTCCCGGCGCATGATC ATTCGGTGGGTAAGGTGGTGGTAACGTTGG GGAAGACAAGCAGACGT-3' (Alexa fluor 488 labelled)	Specific recognition and information encoding ability of DNA aptamers as well as selective absorption and FL quenching of GO.	1–500 ng/mL for both	ZEA: 1.80 ng/mL OTA: 1.48 ng/mL	Wine (91.8–103.6%) [76]
DON	GO	5'-GACATATTCAGTCTGACAGCGTCTTCC CACCTAACTGTCTCCGAGCGCGTTAAAGTC ATCTGATGGACGAATATCGTCTAGC-3'	DON turns-on the FL of FAM-labelled aptamer quenched by GO	200–62500 ng/g	200 ng/g	Oat; wheat flour and corn (84.6–92.6%) [81]
AFB1	AuNPs-GOQDs nanotree	HP1: AACCACGCGCAATCCTAGACT GAGCGCTGGCGTGGGTTGCGCTGATCAAGAC TCCATGA-NH ₂ HP2: CAGCGCTCAGTCTAGGATTCCG CGTGGGTT/i6FAMdT/ TCATGGAGTCTTGATCAGCGCAACCCACGC	Dual signal amplification by dynamic DNA walking on 3D-AuNPs and network hybridization chain reaction of DNA tetrahedron nanostructures on GOQDs	1–1000 pg/mL	0.492 pg/mL	Peanut oil (87.6–105.3%) [71]
PAT, ZEA	GO	PAT: 5'-GCCCCGCAACCCGCATCATCTACACTGATA TTTTACCTT-3' ZEA: 5'-TCATCTATCTATGGTACATTACTATCTGTA ATGTGATATG-3'	PAT and ZEA turn-on the FL of FAM-labelled PAT aptamer and Cy3-labelled ZEA aptamer quenched by GO.	PAT: 0.77–215.8 ng/mL ZEA: 0.32–326.0 ng/mL	PAT: 0.35 ng/mL ZEA: 0.012 ng/mL	Traditional Chinese medicine (84.6–112.7%) [74]

^aIf there is only one value provided in this column, it denotes the LOD value. OTA, ochratoxin A; PAT, patulin; ZEA, zearalenone; FB1, fumonisin B1; AFB1, aflatoxin B1; AFM1, aflatoxin M1; DON, deoxynivalenol; SWCNHs, single-walled carbon nanohorns; cMWCNTs, carboxylic acid-functionalized multi-walled carbon nanotubes; Exfoliated carboxy-GO, exfoliated carboxy-functionalized graphene oxide; rGO/PtNPs micromotors, reduced graphene oxide/platinum nanoparticles based tubular micromotors; rGO/Ni/PtNPs micromotors, reduced graphene oxide/nickel/platinum nanoparticles based tubular micromotors; CeO₂-GOQDs, electrostatically coupled cerium oxide and graphene oxide quantum dots; GO/Fe₃O₄ nanocomposite, graphene oxide and iron oxide nanocomposite; AuNPs-GOQDs nanotree, graphene oxide quantum dots based gold nanoparticles nanotree; HP, hairpin probe; SP, signal probe; FL, fluorescence; EXO III, exonuclease III; FAM, fluorescein amidite or carboxyfluorescein; RhX, rhodamine X; Cy3, cyanine 3 dye; APT and cAPT, aptamer and complementary aptamer; FRET, fluorescence resonance energy transfer; LOD, limit of detection; RSD, LOQ, limit of quantitation; relative standard deviation.

Molinero-Fernandez et al. [69] developed rGO/PtNPs-based tubular micromotors for fluorescent aptasensing with on-off strategy for simultaneous detection of OTA and FB1. Initially, rGO/PtNPs-based tubular micromotors were synthesized rapidly by direct electrodeposition within the conical pores of a polycarbonate template membrane. The detection principle is based on a high-affinity interaction between MYT and its specific aptamer adsorbed on rGO surface resulting in the formation of a conjugate that decreases the fluorescence quenching through minimizing the exposure of aptamer nucleobases to rGO/PtNPs micromotors. However, in the absence of MYTs, the fluorophore-labelled aptamer is adsorbed onto the rGO surface through π - π stacking interactions facilitating the fluorescence quenching. With only 1 μ L of sample, this fluorescence aptasensing assay could rapidly detect both OTA and FB1 within 2 min with an LOD at 7 and 0.4 ng/mL respectively and an LOQ at 10 and 1 ng/mL in the linear range of 1-1000 and 10-1000 ng/mL. Also, a high sensitivity was shown for OTA (95.7 mL/ μ g) and FB1 (589.7 mL/ μ g), while a high accuracy of 96% OTA recovery from wine and 98% FB1 recovery from beer as well as a high precision with RSD at <9% were reported. In a later study, the same authors reported an improved fluorescence aptasensor by incorporating magnetic Ni between rGO and PtNPs [70], with the magnetic rGO/Ni/PtNPs micromotors exhibiting a LOD at 4 ng/mL for OTA and 0.7 ng/mL for FB1 in the linear range of 10–1000 ng/mL for OTA and 5–1000 ng/mL for FB1 as well as a higher accuracy with 104% recovery of FB1 from beer and 105–108% recovery of OTA from wine, implying that a combined adsorption (rGO), magnetic (Ni) and catalytic (PtNPs) properties of rGO/Ni/PtNPs micromotors could facilitate development of more sensitive sensors with accurate control on micromotor operations.

5.1.2. Graphene quantum dots-based fluorescence aptasensors

Unlike the direct fluorescence sensors, sensors developed with fluorescence resonance energy transfer (FRET) technique involves nonradiative phenomenon of energy transfer from an excited donor fluorophore to a ground-state acceptor through intermolecular dipole-dipole coupling [20]. Graphene has attracted great attention for fabrication of FRET-based sensors to quench the fluorescence of many semi-conductor QDs due to its conjugated structure and high quenching efficiency for attaining high sensitivity [66]. Furthermore, the ratiometric FRET strategy represents a simultaneous

measurement of two fluorescence signals at different wavelengths with their ratios being used for quantitation of analytes to attain higher precision [71].

A ratiometric aptamer-based FRET sensor using colloidal cerium oxide nanoparticles (CeO₂-NPs) and GOQDs possessing excellent fluorescence properties was developed by Tian et al. [72] for detection of OTA in peanut. After synthesizing CeO₂-NPs by sol-gel method and GOQDs by pyrolysis, DNA1 and DNA2 oligonucleotides complementary to OTA aptamer were immobilized respectively by chemical bonding and upon mixing DNA1@CeO₂-NPs and DNA2@GOQDs, an electrostatic interaction resulted in the generation of FRET. Also, the addition of OTA aptamer is capable of quenching the FRET and a subsequent incorporation of OTA can recover the FRET for quantitative analysis of OTA. Based on the optimal conditions of pH 7, GOQDs/CeO₂-NPs ratio of 2, aptamer concentration of 100 nM and incubation time of 30 min, a low LOD of 2.5 pg/mL in the linear range of 10–20000 pg/mL with a high selectivity in the presence of AFB1 and ZEA as well as high accuracy with 90–110% recovery from peanut samples were shown. More recently, a fluorescence aptasensor based on dual signal amplification of DNA walker on AuNPs and network hybridization chain reaction (HCR) on DNA tetrahedron nanostructures (DTNs) on GOQDs nanotree was developed for AFB1 detection in food samples [71]. More elaborately, DNA walker, a dynamic DNA nanomachine containing W probe, T probe and energy, was used in this study with W probe capable of walking on 3D-track of AuNPs through energy-induced hybridization or hydrolysis of T-probe for exerting primary signal amplification. The sensitivity of such DNA nanostructures can be further enhanced by HCR which can trigger the formation of hybrid double-strand with two hairpin probes. Also, the network HCR on DNA tetrahedron nanostructures composed of self-assembled four single DNA strands can provide multiple reaction orientations for improved assembly rate of GOQDs nanotree towards triggering secondary signal amplification. This aptasensor was demonstrated to be effective in enhancing sensitivity of AFB1 detection in the linear range of 1–1000 pg/mL at a LOD as low as 0.492 pg/mL with high selectivity even with ZEA, OTA, FB1 and AFM1, as well as a high recovery (87.6–105.3%) from peanut oil.

5.1.3. FRET-based aptasensors with multiplexing capability

Some FRET-based aptasensors with multiplexing capability have been reported recently for detection

of at least two MYTs, which are summarized in the following section. For instance, Wang et al. [73] developed a FRET-based aptasensor for simultaneous detection of AFB1 and FB1 by using GO/Fe₃O₄ nanocomposites as the single energy acceptor with magnetic separation to effectively eliminate background interference for enhanced sensitivity. In addition, AFB1- and FB1-specific aptamers were conjugated respectively with green and red fluorescence emitting CdTe QDs for application as dual energy donors. In the presence of GO/Fe₃O₄, the fluorescence of CdTe QDs was quenched due to π - π stacking interactions between them. However, the addition of sample with AFB1 and FB1 interacted with specific aptamers thereby reducing the contact of aptamer base groups and GO/Fe₃O₄ for recovery of fluorescence and subsequent magnetic separation for analysis. With the optimized incubation time (60 min) and temperature (37 °C), this method showed high detector response towards AFB1 and FB1 over a wide linear range of 0.01–100 ng/mL and 0.05–300 ng/mL respectively with LOD at 6.7 and 16.2 pg/mL. Also, no cross reactivity in the presence of OTA, OTB, AFB2 and AFM1 was reported and the method validation demonstrated high reproducibility (RSD, 5.1–6.3%) and high recovery from peanut samples (92–97%). With an aim to overcome the limitation associated with simultaneous detection of multiple MYTs in traditional Chinese medicine, a rapid, simple and cost-effective FRET-based aptasensing technique was reported in a recent study for dual detection of PAT and ZEA [74]. Specifically, after conjugating fluorescein amidite (FAM)-labeled PAT aptamer and cyanine 3 (Cy3)-labeled ZEA aptamer with GO, followed by addition of PAT and ZEA, a linear fluorescence response in the concentration range of 0.77–215.8 ng/mL and 0.32–326.0 ng/mL was obtained respectively, while a LOD value of 0.35 ng/mL and 0.012 ng/mL as well as a high recovery of 84.6–107.5% and 102.7–112.7% from traditional Chinese medicine with good selectivity in the presence of FB1, T-2, AFG1 and OTA was shown.

5.1.4. Systematic aptamer truncation-based fluorescence aptasensor

Although GO-based aptasensors have been successfully designed and employed for detecting a wide variety of targets, the practical application is limited especially for long aptamers due to their weak output signals and inadequate performance. To remedy this problem, an aptamer truncating strategy was recently reported to be successful by eliminating the extraneous nucleotides and truncating the aptamer length to <40 nucleotides for

enhancement of the aptamer-target binding efficiency [75]. More elaborately, a GO aptasensor was developed by systematically truncating the extraneous nucleotides using circular dichroism as well as binding affinity analysis, and the truncated aptamers of AFB1 and OTA containing 40 and 36 nucleotides respectively were conjugated with GO nanosheets for their simultaneous detection in wine samples. For the AFB1 single-channel aptasensor, the LOD for the truncated AFB1 aptamer (4.8 ng/mL) was 6-fold lower than that without truncation (29.3 ng/mL), while a high recovery ranging from 94.5 to 104.5% in wine samples as well as high selectivity even with AFB1, ZEA, OTA and acetamiprid was attained. But for the AFB1/OTA dual-channel aptasensor, the LOD of AFB1 and OTA was 3.312 and 15.17 ng/mL, respectively and the recovery of both from wine samples ranged from 82.7 to 112.6%, revealing that the developed GO aptasensor with truncated aptamers can be effective for application in real food samples containing multiple MYTs. Moreover, the aptamer truncation strategy is versatile and can be easily applied to other aptamers, opening new ways for designing rapid and low-cost aptasensors with detection capability of multiple MYTs.

5.1.5. Steganography-based fluorescence aptasensor

A GO-based steganographic aptasensor coupled with FRET technique was designed for simultaneous fluorescence detection of ZEA and OTA [76]. It is based on a specific recognition and information encoding ability of DNA aptamers and selective absorption with fluorescence quenching capacity of GO. This steganographic aptasensor acts as an information encryption with GO as cover, aptamers as information carriers for specific target recognition and dual targets (ZEA and OTA) as special keys. Initially, the fluorescence of the aptamers Cy3 and Alexa Fluor 488 is quenched by GO for information encryption and in the presence of ZEA and OTA, their respective aptamers are released from GO surface decrypting the hidden information. Based on this information of encryption/decryption, a simultaneous and sensitive detection of ZEA and OTA can be accomplished. Following optimization of the fluorescence restoration temperature (45 °C), a linear fluorescence response in the concentration range of 1–500 ng/mL was shown for both ZEA and OTA with the LOD at 1.80 and 1.48 ng/mL, respectively. Also, a high selectivity of both MYTs in the presence of AFB1, AFM1, FB1 and PAT was shown with a high recovery of 89.0–99.9% for ZEA and 91.8–103.6% for OTA from wine samples.

5.1.6. Exfoliated functional graphene oxide-based fluorescence aptasensor

Highly water dispersible exfoliated functional GO is adopted as an effective fluorescence quencher of FAM-based fluorescence. Goud et al. [77] synthesized exfoliated carboxy-functionalized GO by ultrasonating GO with sodium hydroxide and chloroacetic acid for 12 h and used for selective aptasensing of ZEA in alcoholic beverages (beer and wine). In the presence of ZEA, an increase in fluorescence intensity due to strong interaction between FAM-labelled aptamer and ZEA showed a linear response in the range of 0.5–64 ng/mL with the LOQ and recovery being 0.5 ng/mL and 87–96% (beer and wine), respectively. Also, a high reproducibility (RSD, 2.4–3.6%) and high selectivity even with OTA, OTB, AFM1, AFB1 and PAT were demonstrated.

5.1.7. Fluorescence polarization-based aptasensor

The FAM-labelled aptamers are usually adsorbed on the surface of GO through π - π stacking and electrostatic interaction forming aptamer/GO macromolecular conjugates that exhibits high fluorescence polarization. However, in the presence of MYTs, the aptamer is dissociated from GO surface and combines with MYT to form aptamer/MYT conjugate, resulting in alteration of the fluorescence polarization caused by change in molecular weight. Based on this principle, Ye et al. [78] developed a low-cost and highly sensitive fluorescence polarization assay for detection of AFB1. With an optimized GO at 50 μ g/mL, aptamer level at 10 nM, detection time at 5 min and pH at 5.4, a linear response of the fluorescence polarization was shown in the range of 0.016–1.56 ng/mL with the LOD at 0.016 ng/mL and AFB1 recovery from rice sample extract ranged from 89.2 to 112%. Also, a highly selective detection of AFB1 was shown even with ZEA, OTA and FB1. Most importantly, this fluorescence polarization-based aptasensor was demonstrated to be superior to GO-based fluorescence quenching assay and direct fluorescence polarization assay without GO.

5.1.8. Other graphene oxide fluorescence aptasensors

In three different studies, the analytical principle involving GO-based fluorescence quenching of FAM-labelled aptamers and turning-on fluorescence with great amplification in the presence of MYT was adopted for detection of OTA, AFM1 and DON respectively in red wine, infant milk powder and oat/wheat flour/corn samples, with the LOD at 0.08 ng/mL, 0.05 ng/g and 200 ng/g as well as recovery ranging from 90.9 to 112%, 92–126% and 84.6–92.6%, respectively [79–81].

5.2. Carbon nanotube/nanohorn-based fluorescence aptasensors

Single-walled carbon nanohorn (SWCNH) is a type of horn-shaped CNM sheath with unique structure of radial formation upon aggregation imparting remarkable properties for use in sensor fabrication [82]. Also, exonuclease III, explored as a DNA-modifying enzyme capable of selectively hydrolyzing a single strand of duplex DNA, was used for cyclic enzymatic digestion of probe DNA in fluorescence autosensing method [83]. By employing SWCNHs and exonuclease III, Wu et al. [84] fabricated a fluorescence aptasensor containing OTA-specific aptamer, exonuclease III as signal amplifier and SWCNHs as fluorescence quenchers for OTA detection. A linear range of 4.04–403.8 ng/mL was shown, with a LOD value of 1.7 ng/mL, reproducibility RSD value of 6.3% and selectivity in the presence of AFB1, FB1, ZEA, OTB, OTC and ZEA. Also, its application to real food samples demonstrated a high OTA recovery from beer (93.8–113.0%) and red wine (92.0–115.9%). In the absence of OTA, the hairpin probe containing OTA-specific aptamer and FAM-labelled signal probe are intact with the fluorescence being quenched by SWCNHs. However, following addition of OTA, the aptamer binds with OTA thereby exposing a single-stranded sequence for both hybridization with signal probe and digestion by the exonuclease III enzyme to release free fluorophore labels for fluorescence aptasensing of OTA.

Given the high fluorescence quenching efficiency, MWCNTs functionalized with carboxylic acid (cMWCNTs) have been widely used for fabrication of fluorescence sensors. More specifically, in a fluorescence aptasensing assay, cMWCNTs being natural electron acceptors facilitate FRET in the presence of an electron donating fluorescence dye-labelled aptamer for enhanced quenching of fluorescence [77]. For example, a switchable fluorescence aptasensor with cMWCNTs was recently developed by Khan et al. [85], who compared three different aptamer sequences and found that the aptamer tagged at 3'-end with 40 nucleotide bases exhibited the maximum affinity towards PAT with high fluorescence recovery. In principle, the FAM-labelled aptamer exhibiting a strong fluorescence can be quenched by cMWCNTs through FRET mechanism and an eventual incubation with PAT solution recovered the fluorescence caused by a conformational change through formation of aptamer-PAT conjugate for measurement. A LOD and LOQ value of 0.13 and 0.41 μ g/mL was obtained respectively in the linear range of 0.005–0.3 ng/mL,

while a high repeatability and reproducibility (RSD, 1.64 and < 4%) as well as high selectivity even with AFB1, OTA, OTB, FB1, ZEA, 5-hydroxymethyl furfural and lactic acid were shown. Application of this method to PAT detection in apple juice showed a high recovery (96.6–98.1%), which is comparable to that obtained by HPLC-ultraviolet-visible spectrometer (UV) method (95.2–98.2%) [85].

6. Miscellaneous carbon nanomaterial-based sensors

Some miscellaneous carbon nanomaterial-based sensors were also reported recently for MYT analysis in food, which include colorimetry, fluorometry and surface enhanced Raman spectroscopy (SERS) based sensors as well as electrochemical sensors without specific recognition element and with MIPs (Table 6).

6.1. Colorimetric sensor

A pH-resolved Colorimetry was developed by Hao et al. [86] for simultaneous detection of AFB1, OTA, FB1 and MC-LR using allochroic dyes malachite green carbinol base (MGCB), phenolphthalein (PP), thymolphthalein (TP) and methyl violet (MV), respectively. Incorporation of the respective mycotoxin aptamer facilitated self-assembling of two GO platforms which were respectively tagged with DNA probe 1 plus dyes and DNA probe 2 plus Fe₃O₄. The presence of MYTs dissociated the self-assembly enriching the corresponding dye color in solution. After biorecognition and magnetic separation, the solution pH was adjusted by adding acidic or alkaline water to control the release of dyes from GO. More specifically, the acidic condition turned the supernatant color to a mixture of green (MGCB) and purple (MV) for analysis of AFB1 (617 nm) and MC-LR (570 nm) respectively, while the alkaline condition changed the precipitate color to a mixture of pink (PP) and blue (TP) enabling analysis of OTA (552 nm) and FB1 (594 nm). This colorimetric optical sensor was shown to be effective in multiplex analysis of 4 MYTs with high selectivity in a wide linear range of 5–250 ng/mL and the application to peanut samples demonstrated a high recovery of 97.8–104.3%.

6.2. Fluorometric sensor

As an analogue of 2D-inorganic graphene, graphitic carbon nitride has gained attention due to their superior optoelectronic properties as well as large specific surface area, excellent

biocompatibility and high water dispersibility [87]. Also, the incorporation of polymer such as β -cyclodextrin possessing abundant hydroxyl groups can not only enable functionalization of fluorescent probes, but also adsorb analytes by host–guest interaction for effective modulation of fluorescent signals [88]. However, β -cyclodextrin possesses weak specific recognition ability especially in complex sample matrix, which can be solved by synthesizing MIPs with β -cyclodextrin [89]. This in turn overcomes the limitation of conventional molecular imprinting technique such as difficulty in template elution, poor water solubility, and slow mass transfer rate. In light of this strategy, Shi et al. [90] developed a fluorometric probe for detection of sterigmatocystin (SMC) by MIP-coated- β -cyclodextrin functionalized graphitic carbon nitride nanosheets (MIP@ β CD/CNNS) and reported high fluorescence quantum yield (13%), high SMC adsorption capacity (86 mg/g), faster adsorption rate (25 min) and good adsorption selectivity in the presence of biotoxins, amino acids, vitamins, starches, and metal ions in wheat. Based on the FRET principle, the SMC was detected through quenching of the blue fluorescence of MIP@ β CD/CNNS (excitation/emission wavelength at 368/432 nm) by MIP@ β CD/CNNS with the LOD at 24 ng/mL in the linear range of 48.65–1005.3 ng/mL. Application to SMC-spiked wheat extracts (50, 100 and 200 ng/g) showed a high recovery ranging from 95.5 to 100.4% with RSD at 1.4–3.2%.

6.3. SERS-based sensor

SERS is emerging as a powerful technique in the field of food science and technology especially for food inspection [91,92]. In principle, it enhances the Raman signals through adsorption of analytes close to the vicinity of localized surface plasmon resonance (hot spots) generated by metal nanostructures depending on the variation in their roughness [93,94]. Moreover, the integration of an engineered plasmonic nanostructure with other functional materials enables a synergistic modulation of both chemical and electromagnetic properties of the hybrid substrate for efficient SERS analysis [95]. The substrates with surface patterns composed of vertically inclined pillar-like structures with high aspect ratio, rough sidewalls and sharp tips can provide further enhancement in Raman signals for attaining highly sensitive SERS analysis. For instance, Santhosh et al. [96] fabricated a gold-film coated branched vertical CNTs with 70–80 nm in thickness and 2 μ m in height for determination of 4 MYTs including AFB1, ZEA, alternariol and FB1. An

Table 6. Miscellaneous carbon nanomaterial-based methods developed recently for MYT analysis in food.

Mycotoxin	Carbon nanomaterial	Detection method	Probe/principle	Linear range	LOD	Method reproducibility RSD; Application (Recovery)	Reference
AFB1, OTA, FB1, MC-LR	GO and Fe ₃ O ₄ /GO	Colorimetric biosensor	MYTs dissociated the self-assembly of DNA probe 1+GO-dyes and DNA probe 2+ Fe ₃ O ₄ /GO in acidic condition giving green color for AFB1 and purple for MC-LR, while in alkaline pink color for OTA and blue for FB1.	5–250 ng/mL	5–10 ng/mL	3.2–7.2%; peanut (97.8–104.3%)	[86]
ZEA	SWCNTs	Electrochemical (DPV, EIS, CV)	A direct voltammetric method by coating SWCNTs on CSPE	7.96–318.4 ng/mL	0.318 ng/mL	4.6%; corn flake (98.6–103.3%)	[97]
SMC	MIP@βCD/CNNS	Fluorometry	With CNNS acting as chromophore as well as βCD and MIP as recognition groups, the blue fluorescence of MIP@βCD/CNNS is quenched by SMC.	48.65–1005.3 ng/mL	24 ng/mL	1.4–3.2%; wheat (95.5–100.4%)	[90]
AFB1	AuNPs-GQDs	Electrochemical (LSV, EIS)	A direct voltammetric method by coating AuNPs-GQDs on SPE	0.329–16.46 ng/mL	0.155 ng/mL	7.5%; malted barley (76–103%)	[99]
ZEA	GR/PLA filaments	Electrochemical (CV)	Chemical and electrochemical activation of 3D printed GR/PLA removed the PLA filaments exposing the inner GR surface for sensitive detection	3.18–95.51 mg/L	0.108 mg/L	–	[98]
DON	PLR-MIP@cMWCNTs	Electrochemical (DPV, CV)	Signal enhancement due to high conductivity of PLR, high surface area of MWCNTs and antibody-like DON recognition of MIP.	29.6–20742 ng/mL	20.7 ng/mL	1.8%; wheat flour (85.1–86.6%)	[101]
AFB1, ZEA, FB1, alternariol	Vertical/branched MWCNTs@Au film	SERS	An enhancement factor of 5×10^7 was due to the roughness and high aspect ratio of vertical and pillar-like structures of MWCNTs.	AFB1: 3.29–3291.5 ng/mL ZEA: 3.18–3183.6 ng/mL FB1: 7.22–7218.3 ng/mL ALT: 2.58–2582.3 ng/mL	AFB1: 3.29 ng/mL ZEA: 3.18 ng/mL FB1: 7.22 ng/mL ALT: 2.58 ng/mL	–	[96]

AFB1, aflatoxin B1; OTA, ochratoxin A; ZEA, zearalenone; FB1, fumonisin B1; MC-LR, microcystin-LR; SMC, sterigmatocystin; DON, deoxynivalenol; GO, graphene oxide; Fe₃O₄/GO, nanocomposite of graphene oxide and iron oxide; SWCNTs, single-walled carbon nanotubes; MWCNTs, multi-walled carbon nanotubes; MIP@βCD/CNNS, MIP-coated β-cyclodextrin functionalized graphitic carbon nitride nanosheets; AuNPs-GQDs, nanocomposite of gold nanoparticles and graphene quantum dots; GR/PLA filaments, graphene/poly(lactic acid) filaments; Vertical/branched MWCNTs@Au, gold-film coated vertical and branched MWCNTs; PLR-MIP@cMWCNTs, poly(L-arginine) electropolymerized molecularly imprinted polymer on carboxylated MWCNTs; PLA, poly(lactic acid); PLR, poly(L-arginine); CV, cyclic voltammetry; DPV, differential pulse voltammetry; EIS, electrochemical impedance spectroscopy; LSV, linear sweep voltammetry; SERS, surface enhanced Raman spectroscopy; CSPE, carbon screen-printed electrode; SPE, screen printed electrode; LOD, limit of detection; RSD, relative standard deviation.

enhancement factor of 5×10^7 was shown for Raman signals at 633 nm with the linear range and LOD respectively from 3.29 to 3291.5 ng/mL and 3.29 ng/mL for AFB1, 3.18–3183.6 ng/mL and 3.18 ng/mL for ZEA, 7.22–7218.3 ng/mL and 7.22 ng/mL for FB1, and 2.58–2582.3 ng/mL and 2.58 ng/mL for alternariol. In this study, a highly stable CNTs in clusters with controllable thickness was successfully prepared in the presence of a nickel catalyst by employing a fast and facile radio frequency-based inductively coupled plasma-enhanced chemical vapor deposition [96].

6.4. Electrochemical sensors without specific recognition elements

In an attempt to develop a fast, reliable and direct voltammetric method without specific recognition elements such as antibody, aptamer or MIPs, Radi et al. [97] reported a 3-fold enhancement of CSPE oxidation peak current for ZEA in an adsorption stripping-based DPV method after coating CSPE with SWCNTs. With an optimized pH at 7.0 and scan rate at 100 mV/s for ZEA concentration at 1×10^{-5} M, an LOD value of 0.318 ng/mL was obtained for a linear anodic peak current response for ZEA level ranging from 7.96 to 318.40 ng/mL. Also, a high precision (RSD, 4.6%) and high selectivity in the presence of FB1, FB2 and DON was shown with high stability retaining 95% signal response even after 50 CV cycles over a 10-day testing period. By spiking 5 different concentrations (10–200 µg/L), ZEA with a mean recovery from 98.6 to 103.3% was obtained from corn flake extracts, demonstrating a successful application of SWCNTs owing to their favorable surface functional orientation towards ZEA, high electrochemically active area and efficient electron transfer properties. This method was claimed to minimize electrode fouling after successive analysis for longer duration without requiring any complicated pretreatment step [97].

Later, Nasir et al. [98] fabricated a 3D-printed graphene electrode by fused deposition modelling using graphene/polylactic acid filaments. Briefly, graphene/polylactic acid filaments were activated chemically by soaking in DMF for 10 min, followed by sequentially washing with ethanol and water, drying overnight and electrochemically activating with 0.01 M PBS under an electric potential of 2.5 V against Ag/AgCl reference electrode. Both chemical and electrochemical activation could effectively remove the external polylactic acid layers exposing graphene for enhanced sensitivity for ZEA detection in the linear range of 3.18–95.51 mg/L with the LOD and LOQ at 0.108 and 0.360 mg/L respectively.

However, this study fails to verify interference effects and apply to real food samples. For future study, the exploration of a better design of 3D-printed graphene electrodes, functionalization of graphene surface and choice of alternative conductive materials like transition metal dichalcogenides for modification are necessary to develop an improved electrochemical sensor for MYTs. In another study, a nanocomposite of AuNPs and GQDs synthesized by citric acid pyrolysis method was used to fabricate SPE for voltammetric determination of AFB1 in malted barley [99]. With an optimized pH at 5, applied potential at -0.2 V and accumulation time for AFB1 oxidation at 90 s, the AuNPs-GQDs nanocomposite coated on SPE was shown to provide a linear response in the concentration range of 0.329–16.46 ng/mL, with the LOD and LOQ being 0.155 and 0.468 ng/mL, respectively. Moreover, a high repeatability (RSD, 3.1%) and reproducibility (RSD, 7.5%) as well as 76–103% recovery from malted barley was reported, demonstrating an insignificant matrix effect and successful application of this electrochemical method as a non-biological alternative (without antibody or aptamer) for AFB1 determination in food.

6.5. Electrochemical sensor with molecular imprinted polymers

As most electrochemical immunosensors involves expensive antibody biorecognition element and are susceptible to various environmental factors such as pH and temperature, low-cost biomimetic sensors with higher life span and immunosensor-like characteristics are recently developed [22]. In recent years, the application of highly selective MIPs as a specific recognition element mimicking antibodies have been shown to enhance the stability and life span of sensors [4]. It is worth pointing out that the molecularly imprinting technique provides good control on film thickness as well as uniform and well-adherent coating [19]. Moreover, the employment of electropolymerization technique for simultaneous polymerization and deposition of polymer on the electrode and incorporation of carbon nanomaterials can impart excellent sensitivity to the electrochemical biosensors [100]. By electropolymerizing a biodegradable poly(L-arginine) (PLR) on cMWCNTs coated GCE through peptide-bond formation, Li et al. [101] developed PLR-MIP@cMWCNTs for detection of DON and demonstrated a high conductivity, large surface area, antibody-like molecular recognition with a linear response ranging from 29.6 to 20742 ng/mL and LOD at 20.7 ng/mL in wheat flour samples.

Moreover, this biomimetic sensor was highly reproducible (RSD, 1.8%) with stable signals up to 30 cycles and highly selective even with OTA, ZEA, essential metals, glucose and sucrose. Also, a high recovery ranging from 85.1 to 86.8% was reported in wheat flour, which was comparable to that obtained by HPLC method (83.7–84.6%) [101].

7. Conclusion and future perspective

In conclusion, recent trends on MYT analysis in food by employing various CNMs such as CNTs, GR/GO/rGO and their nanocomposites with polymer and/or metal and metal oxide nanoparticles were overviewed. The application of CNMs as SPE and dSPE adsorbents to increase the enrichment efficiency of MYTs in liquid chromatographic methods has facilitated simultaneous analysis of 6–20 MYTs with high sensitivity, acceptable recovery and high reproducibility by reducing the matrix effect and eliminating the sample pretreatment step. However, there is an urgent need to control the aggregation property of CNMs through appropriately tailored surface functionalization which can not only improve the enrichment efficiency for MYTs, but also increase their regeneration/reuse capability. Also, novel CNMs with high surface area, high adsorption efficiency and excellent reusability should be synthesized by adopting low-cost and green synthesis methods. Application of functionalized CNTs or graphene materials as coating material for conventional electrodes in electrochemical sensors enabled flexibility in functionalization and high immobilization of specific recognition elements (antibody, aptamer or MIPs) for analyzing MYTs in a broad linear range and low LOD at picogram level with high selectivity, accuracy and reproducibility. Moreover, by exploring the fluorescence quenching property of CNMs, various fluorescence aptasensors developed recently are able to analyze MYTs with high sensitivity in a variety of food matrices. Thus, through simplified procedure, miniature design and portability, the reported CNM-based electrochemical and optical sensors can shorten the analysis time and sample volume without compromising sensitivity of MYTs in food.

Although the electrochemical and optical sensing methods developed so far for MYT analysis are successfully demonstrated at the laboratory scale, they are still not commercially available for wide practical application due to complicated electrode modification procedure, short life-time/low stability of fluorophores used in fluorescence sensors and incapability to analyze multi-MYTs. These

limitations can be overcome by using simple and novel recombinant antibody or aptamer with good performance at natural conditions, exploring the use of fluorescent nanoparticles as label probes in affinity-based assays and engineering the nanomaterials with novel surface chemistry for fabrication of label-free sensors with multiplexing capability. In addition, the application of these sensors is mostly restricted to analysis of certain specific MYTs such as AFB1, OTA, ZEA, PAT, AFM1 and DON, and thus some other MYTs should be also be investigated. Development of a large number of ratiometric sensors with dual signals is necessary to improve both sensitivity and accuracy of MYT analysis in food. The other technical issues need to be overcome include poor resistance to interfering compounds and electrode fouling in electrochemical sensors as well as complex fluorescence labeling steps, autofluorescence and bleaching of fluorescent signal labels in fluorescence sensors. The future studies can also be directed to integration of nanomaterial-based sensor with microfluidics for lab-on-chip device development and smartphone-based microfluidic sensor.

Conflict of interest

The authors have no conflicts of interest to declare.

References

- [1] European Union (EU). White paper on Food Safety, Commission of the European Communities, Brussels, 2000. Accessed at <http://ec.europa.eu/dgs/health.consumer/library/pub/pub06.en.pdf>.
- [2] Chen BH, Inbaraj BS. Nanomaterial-based sensors for mycotoxin analysis in food. In: Grumezescu AH, editor. *Nanoscience and food industry*. USA: Elsevier; 2016. p. 387–423.
- [3] Goud KY, Kailasa SK, Kumar V, Tsang YF, Lee SE, Gobi KV, et al. Progress on nanostructured electrochemical sensors and their recognition elements for detection of mycotoxins: a review. *Biosens Bioelectron* 2018;121:205–22.
- [4] Le VT, Vasseshian Y, Dragoi EN, Moradi M, Khaneghah AM. A review on graphene-based electrochemical sensor for mycotoxins detection. *Food Chem Toxicol* 2021;148:111931.
- [5] Zhang X, Li G, Wu D, Liu J, Wu Y. Recent advances on emerging nanomaterials for controlling the mycotoxin contamination: from detection to elimination. *Food Front* 2020;1:360–81.
- [6] Bhat R, Rai RV, Karim AA. Mycotoxins in food and feed: present status and future concerns. *Compr Rev Food Sci Food Saf* 2010;9:57–81.
- [7] Claeys L, Romano C, Ruyck KD, Wilson H, Fervers B, Korenjak M, et al. Mycotoxin exposure and human cancer risk: a systematic review of epidemiological studies. *Compr Rev Food Sci Food Saf* 2020;19:1449–64.
- [8] International Agency for Research on Cancer (IARC). *Monograph on the evaluation of carcinogenic risk to humans*, vol. 82. Lyon: World Health Organization; 2002. p. 171.

- [9] Ostry V, Malir F, Toman J, Grosse Y. Mycotoxins as human carcinogens – the IARC monographs classification. *Mycotoxin Res* 2017;33:65–73.
- [10] Ma S, Wang M, You T, Wang K. Using magnetic multi-walled carbon nanotubes as modified QuEChERS adsorbent for simultaneous determination of multiple mycotoxins in grains by UPLC-MS/MS. *J Agric Food Chem* 2019;67:8035–44.
- [11] Janik E, Niemcewicz M, Ceremuga M, Stela M, Saluk-Bijak J, Siadkowski A, et al. Molecular aspects of mycotoxins – a serious problem for human health. *Int J Mol Sci* 2020;21:8187.
- [12] European Commission (EC). Commission regulation EU No 165/2010 of 26 February 2010 amending Regulation EC No 1881/2006 setting maximum levels for certain contamination in foodstuffs as regards aflatoxin. *Off J Eur Union L* 2010;50:8–12.
- [13] United States Food and Drug Administration (USFDA). *Inventory of effective food contact substance (FCS)*. Notification No. 178. 2002. Retrieved from.
- [14] Singh J, Mehta A. Rapid and sensitive detection of mycotoxins by advanced and emerging analytical methods: a review. *Food Sci Nutr* 2020;8:2183–204.
- [15] Aoac International. AOAC official methods. 2000. Gaithersburg, MD.
- [16] Brera C, Debnaghn F, Minardi V, Pannunzi E, De Santis B, Miraglia M, et al. Immunoaffinity column cleanup with liquid chromatography for determination of aflatoxin B1 in corn samples: interlaboratory study. *J AOAC Int* 2007;90:765–72.
- [17] Malhotra BD, Srivastava S, Ali MA, Chandan S. Nanomaterial-based biosensors for food toxin detection. *Appl Biochem Biotechnol* 2014;174:880–96.
- [18] Inbaraj BS, Chen BH. Nanomaterial-based sensors for detection of foodborne bacterial pathogens and toxins as well as pork adulteration in meat products. *J Food Drug Anal* 2016;24:15–28.
- [19] Goud KY, Reddy KK, Satyanarayana M, Kummari S, Gobi KV. A review on recent developments in optical and electrochemical aptamer-based assays for mycotoxins using advanced nanomaterials. *Microchim Acta* 2020;187:29.
- [20] Sharma A, Khan R, Catanante G, Sherazi TA, Bhand S, Hayat A, et al. Designed strategies for fluorescence-based biosensors for the detection of mycotoxins. *Toxins* 2018;10:197.
- [21] Asadian E, Ghalkhani M, Shahrokhian S. Electrochemical sensing based on carbon nanoparticles: a review. *Sens Actuators, B* 2019;293:183–209.
- [22] Ma X, Li X, Zhang W, Meng F, Wang X, Qin Y, et al. Carbon-based nanocomposite smart sensors for the rapid detection of mycotoxins. *Nanomaterials* 2021;11:2851.
- [23] Chen X, Wu H, Tang X, Zhang Z, Li P. Recent advances in electrochemical sensors for mycotoxin detection in food. *Electroanalysis* 2021;33:1–11.
- [24] Jiang K, Huang Q, Fan K, Wu L, Nie D, Guo S, et al. Reduced graphene oxide and gold nanoparticle composite-based solid-phase extraction coupled with ultra-high-performance liquid chromatography-tandem mass spectrometry for the determination of 9 mycotoxins in milk. *Food Chem* 2018;264:218–25.
- [25] Li N, Qiu J, Qian Y. Amphiphilic block copolymer-grafted magnetic multi-walled carbon nanotubes as QuEChERS adsorbent for simultaneous determination of mycotoxins and pesticides in grains via liquid chromatography tandem mass spectrometry. *Microchim Acta* 2020;187:648.
- [26] Li N, Qiu J, Qian Y. Polyethyleneimine-modified magnetic carbon nanotubes as solid-phase extraction adsorbent for the analysis of multi-class mycotoxins in milk via liquid chromatography-tandem mass spectrometry. *J Separ Sci* 2021;44:636–44.
- [27] Augusto F, Hantao LW, Mogollón NG, Braga SC. New materials and trends in sorbents for solid-phase extraction. *Trends Anal Chem* 2013;43:14–23.
- [28] Zhao Y, Yuan YC, Bai XL, Liu YM, Wu GF, Yang FS, et al. Multi-mycotoxins analysis in liquid milk by UHPLC-Q-Exactive HRMS after magnetic solid-phase extraction based on PEGylated multi-walled carbon nanotubes. *Food Chem* 2020;305:125429.
- [29] Jiang K, Huang P, Luan L, Fan K, Guo W, Zhao Z, et al. Iron (II, III) oxide/multi-walled carbon nanotube composite as solid-phase extraction sorbent followed by ultra-high performance liquid chromatography tandem mass spectrometry for simultaneous determination of zearalenone and type A trichothecenes in *Salviae miltiorrhizae* Radix et Rhizoma (Danshen). *J Chromatogr A* 2017;1482:1–10.
- [30] Tanveer ZI, Huang Q, Liu L, Jiang K, Nie D, Pan H, et al. Reduced graphene oxide-zinc oxide nanocomposite as dispersive solid-phase extraction sorbent for simultaneous enrichment and purification of multiple mycotoxins in *Coptidis rhizoma* (Huanglian) and analysis by liquid chromatography tandem mass spectrometry. *J Chromatogr A* 2020;1630:461515.
- [31] Bobrinetskiy I, Knezevic NZ. Graphene-based biosensors for on-site detection of contaminants in food. *Anal Methods* 2018;10:5061–70.
- [32] Xie J, Fang X, Dai X, Shao B, Li J, Jiang Y, et al. Antibody-functionalized reduced graphene oxide films for highly selective capture and purification of aflatoxins. *Microchim Acta* 2019;186:193.
- [33] Eivazzadeh-Keihan R, Pashazadeh P, Hejazi M, Guardia ML, Mokhtarzadeh A. Recent advances in Nanomaterial-mediated Bio and immune sensors for detection of aflatoxin in food products. *Trends Anal Chem* 2017;87:112–28.
- [34] Li R, Wen Y, Wang F, He P. Recent advances in immunoassays and biosensors for mycotoxins detection in feedstuffs and foods. *J Anim Sci Biotechnol* 2021;12:108.
- [35] Azri FA, Selamat J, Sukor R. Electrochemical immunosensor for the detection of aflatoxin B1 in palm kernel cake and feed samples. *Sensors* 2017;17:2776.
- [36] Azri FA, Sukor R, Selamat J, Abu Bakar F, Yusof NA, Hajian R. Electrochemical immunosensor for detection of aflatoxin B₁ based on indirect competitive ELISA. *Toxins* 2018;10:196.
- [37] Bhardwaj H, Pandey MK, Rajesh Sumana G. Electrochemical Aflatoxin B1 immunosensor based on the use of graphene quantum dots and gold nanoparticles. *Microchim Acta* 2019;186:592.
- [38] Bhardwaj H, Marquette CA, Dutta P, Rajesh Sumana G. Integrated graphene quantum dot decorated functionalized nanosheet biosensor for mycotoxin detection. *Anal Bioanal Chem* 2020;412:7029–41.
- [39] Xu W, Qing Y, Chen S, Chen J, Qin Z, Qiu JF, et al. Electrochemical indirect competitive immunoassay for ultra-sensitive detection of zearalenone based on a glassy carbon electrode modified with carboxylated multi-walled carbon nanotubes and chitosan. *Microchim Acta* 2017;184:3339–47.
- [40] Migliorini FL, dos Santos DM, Soares AC, Mattoso LHC, Oliveira ON, Correa DS. Design of a low-cost and disposable paper-based immunosensor for the rapid and sensitive detection of aflatoxin B1. *Chemosensors* 2020;8:87.
- [41] Zhang X, Liao X, Wu Y, Xiong W, Du J, Tu Z, et al. A sensitive electrochemical immunosensing interface for label-free detection of aflatoxin B1 by attachment of nanobody to MWCNTs-COOH@black phosphorene. *Anal Bioanal Chem* 2022;414:1129–39.
- [42] Costa MP, Frías IAM, Andrade CAS, Oliveira MDL. Impedimetric immunoassay for aflatoxin B1 using a cysteine modified gold electrode with covalently immobilized carbon nanotubes. *Microchim Acta* 2017;184:3205–13.
- [43] Riberi WI, Zon MA, Fernández H, Arévalo FJ. Impedimetric immunosensor to determine patulin in apple juices using a glassy carbon electrode modified with graphene oxide. *Microchem J* 2020;158:105192.
- [44] Liu N, Nie D, Tan Y, Zhao Z, Liao Y, Wang H, et al. An ultrasensitive amperometric immunosensor for

- zearalenones based on oriented antibody immobilization on a glassy carbon electrode modified with MWCNTs and AuPt nanoparticles. *Microchim Acta* 2017;184:147–53.
- [45] Riberi WI, Tarditto LV, Zon MA, Arévalo FJ, Fernández H. Development of an electrochemical immunosensor to determine zearalenone in maize using carbon screen printed electrodes modified with multi-walled carbon nanotubes/polyethyleneimine dispersions. *Sens Actuators, B* 2018;254:1271–7.
- [46] Huang Y, Zhu F, Guan J, Wei W, Zou L. Label-free amperometric immunosensor based on versatile carbon nanofibers network coupled with Au nanoparticles for aflatoxin B1 detection. *Biosensors* 2021;11:5.
- [47] Abera BD, Falco A, Ibba P, Cantarella G, Petti L, Lugli P. Development of flexible dispense-printed electrochemical immunosensor for aflatoxin M1 detection in milk. *Sensors* 2019;19:3912.
- [48] Abera BD, Shkodra B, Douaki A, Ibba P, Cantarella G, Petti L, et al. Single-walled carbon nanotube-coated flexible and soft screen-printed electrochemical biosensor for ochratoxin A detection. *IEEE Int Symp Circuits Systems (ISCAS)* 2020:1–5.
- [49] Sharifuzzaman M, Barman SC, Zahed MA, San NJ, Park JY. Green synthesis of reduced graphene oxide decorated with few-layered MoS₂-nanoroses and Au/Pd/Ag trimetallic nanoparticles for ultrasensitive label-free immunosensing platforms. *J Electrochem Soc* 2019;166:B249–57.
- [50] Kudr J, Zhao L, Nguyen EP, Arola H, Nevanen TK, Adam V, et al. Inkjet-printed electrochemically reduced graphene oxide microelectrode as a platform for HT-2 mycotoxin immunoenzymatic biosensing. *Biosens Bioelectron* 2020;156:112109.
- [51] Song X, Wang D, Kim M. Development of an immuno-electrochemical glass carbon electrode sensor based on graphene oxide/gold nanocomposite and antibody for the detection of patulin. *Food Chem* 2021;342:128257.
- [52] Qileng A, Huang S, He L, Qin W, Liu W, Xu Z, et al. Composite films of CdS nanoparticles, MoS₂ nanoflakes, reduced graphene oxide, and carbon nanotubes for ratiometric and modular immunosensing-based detection of toxins in cereals. *ACS Appl Nano Mater* 2020;3:2822–9.
- [53] Evtugyn G, Hianik T. Electrochemical immune- and aptasensors for mycotoxin determination. *Chemosensors* 2019;7:10.
- [54] Yang F, Wang P, Wang R, Zhou Y, Su X, He Y, et al. Label free electrochemical aptasensor for ultrasensitive detection of ractopamine. *Biosens Bioelectron* 2016;77:347–52.
- [55] Jo EJ, Mun H, Kim SJ, Shim WB, Kim MG. Detection of ochratoxin a (OTA) in coffee using chemiluminescence resonance energy transfer (CRET) aptasensor. *Food Chem* 2016;194:1102–7.
- [56] Abnous K, Danesh NM, Alibolandi M, Ramezani M, Taghdisi SM. Amperometric aptasensor for ochratoxin A based on the use of a gold electrode modified with aptamer, complementary DNA, SWCNTs and the redox marker methylene blue. *Microchim Acta* 2017;184:1151–9.
- [57] Wang X, Sun G, Routh P, Kim DH, Huang W, Chen P. Heteroatom-doped graphene materials: syntheses, properties and application. *Chem Soc Rev* 2014;43:7067–98.
- [58] Tian H, Wang L, Sofer Z, Pumera M, Ronanni A. Doped graphene for DNA analysis: the electrochemical signal is strongly influenced by the kind of dopant and the nucleobase structure. *Sci Rep* 2016;6:33046.
- [59] Tian H, Sofer Z, Pumera M, Bonanni A. Investigation on the ability of heteroatom-doped graphene for biorecognition. *Nanoscale* 2017;9:3530–6.
- [60] Luo L, Ma S, Li L, Liu X, Zhang J, Li X, et al. Monitoring zearalenone in corn flour utilizing novel self-enhanced electrochemiluminescence aptasensor based on NGQDs-NH₂-Ru@SiO₂ luminophore. *Food Chem* 2019;292:98–105.
- [61] Sangu SS, Abdul Karim NAM, Saheed MSM, Gopinath SCB. Highly sensitive aptasensor based on 'rose petal' shaped iron nanoparticles decorated on 3D graphene for detection of zearalenone. *IOP Conf Ser Earth Environ Sci* 2021;842:012016.
- [62] Ong CC, Sangu SS, Illias NM, Gopinath SCB, Saheed MSM. Iron nanoflorets on 3D-graphene-nickel: a 'Dandelion' nanostructure for selective deoxynivalenol detection. *Biosens Bioelectron* 2020;154:112088.
- [63] Wang P, Wang L, Ding M, Pei M, Guo W. Ultrasensitive electrochemical detection of ochratoxin A based on signal amplification by one-pot synthesized flower-like PEDOT–AuNFs supported on a graphene oxide sponge. *Analyst* 2019;144:5866–74.
- [64] Lin T, Shen Y. Fabricating electrochemical aptasensors for detecting aflatoxin B1 by layer-by-layer self-assembly. *J Electroanal Chem* 2020;870:114247.
- [65] Nekrasov N, Jaric S, Kireev D, Emelianov AV, Orlov AV, Gadjanski I, et al. Real-time detection of ochratoxin A in wine through insight of aptamer conformation in conjunction with graphene field-effect transistor. *Biosens Bioelectron* 2022;200:113890.
- [66] Li Y, Liu D, Zhu C, Shen X, Liu Y, You T. Sensitivity programmable ratiometric electrochemical aptasensor based on signal engineering for the detection of aflatoxin B1 in peanut. *J Hazard Mater* 2020;387:122001.
- [67] Mu Z, Ma L, Wang J, Zhou J, Yuan Y, Bai L. A target-induced amperometric aptasensor for sensitive zearalenone detection by CS@AB-MWCNTs nanocomposite as enhancers. *Food Chem* 2021;340:128128.
- [68] Krishnan SK, Singh E, Singh P, Meyyappan M, Nalwa HS. A review on graphene-based nanocomposites for electrochemical and fluorescent biosensors. *RSC Adv* 2019;9:8778–881.
- [69] Molinero-Fernández A, Moreno-Guzmán M, López MA, Escarpa A. Biosensing strategy for simultaneous and accurate quantitative analysis of mycotoxins in food samples using unmodified graphene micromotors. *Anal Chem* 2017;89:10850–7.
- [70] Molinero-Fernández A, Jodra A, Moreno-Guzmán M, López MA, Escarpa A. Magnetic reduced graphene oxide/nickel/platinum nanoparticles micromotors for mycotoxin analysis. *Chemistry–Eur J* 2018;24:7172–6.
- [71] Wang Q, Zhao F, Yang Q, Wu W. Graphene oxide quantum dots based nanotree illuminates AFB1: dual signal amplified aptasensor detection AFB1. *Sens Actuators, B* 2021;345:130387.
- [72] Tian J, Wei W, Wang J, Ji S, Chen G, Lu J. Fluorescence resonance energy transfer aptasensor between nanoceria and graphene quantum dots for the determination of ochratoxin A. *Anal Chim Acta* 2018;1000:265–72.
- [73] Wang C, Huang X, Tian X, Zhang X, Yu S, Chang X, et al. A multiplexed FRET aptasensor for the simultaneous detection of mycotoxins with magnetically controlled graphene oxide/Fe₃O₄ as a single energy acceptor. *Analyst* 2019;144:6004–10.
- [74] Zhang N, Li J, Liu B, Wang H, Zhang D, Li Z. A facile "turn-on" fluorescent aptasensor for simultaneous detection of dual mycotoxins in traditional Chinese medicine based on graphene oxide and FRET. *Toxicon* 2022;206:42–50.
- [75] Wang X, Gao X, He J, Hu X, Li Y, Li X, et al. Systematic truncating of aptamers to create high-performance graphene oxide (GO)-based aptasensors for the multiplex detection of mycotoxins. *Analyst* 2019;144:3826–35.
- [76] Wang Q, Yang Q, Wu W. Graphene-based steganographic aptasensor for information computing and monitoring toxins of biofilm in food. *Front Microbiol* 2020;10:3139.
- [77] Goud KY, Hayat A, Satyanarayana M, Kumar VS, Catanante G, Gobi KV, et al. Aptamer-based zearalenone assay based on the use of a fluorescein label and a functional graphene oxide as a quencher. *Microchim Acta* 2017;184:4401–8.
- [78] Ye H, Lu Q, Duan N, Wang Z. GO-amplified fluorescence polarization assay for high-sensitivity detection of aflatoxin B₁ with low dosage aptamer probe. *Anal Bioanal Chem* 2019;411:1107–15.

- [79] Ma C, Wu K, Zhao H, Liu H, Wang K, Xia K. Fluorometric aptamer-based determination of ochratoxin A based on the use of graphene oxide and RNase H-aided amplification. *Microchim Acta* 2018;185:347.
- [80] Guo X, Wen F, Qiao Q, Zheng N, Saive M, Fauconnier ML, et al. A novel graphene oxide-based aptasensor for amplified fluorescent detection of aflatoxin M₁ in milk powder. *Sensors* 2019;19:3840.
- [81] Qin M, Zhang X, Zhao X, Song Y, Zhang J, Xia X, et al. Complementary chain competition and fluorescence quenching detection of deoxynivalenol and analytical applications using a novel aptamer. *CyTA - J Food* 2021;19:257–64.
- [82] Lv L, Cui CB, Liang CY, Quan WR, Wang SH, Guo ZJ. Aptamer-based single-walled carbon nanohorn sensors for ochratoxin A detection. *Food Control* 2016;60:296–301.
- [83] Zhao Y, Liu R, Sun W, Lv L, Guo Z. Ochratoxin A detection platform based on signal amplification by exonuclease III and fluorescence quenching by gold nanoparticles. *Sensor Actuator B Chem* 2018;255:1640–5.
- [84] Wu H, Liu R, Kang X, Liang C, Lv L, Guo Z. Fluorometric aptamer assay for ochratoxin A based on the use of single walled carbon nanohorns and exonuclease III-aided amplification. *Microchim Acta* 2018;185:27.
- [85] Khan R, Sherazi TA, Catanante G, Rasheed S, Marty JL, Hayat A. Switchable fluorescence sensor toward PAT via CA-MWCNTs quenched aptamer-tagged carboxy-fluorescein. *Food Chem* 2020;312:126048.
- [86] Hao N, Lu J, Zhou Z, Hua R, Wang K. A pH-resolved colorimetric biosensor for simultaneous multiple target detection. *ACS Sens* 2018;3:2159–65.
- [87] Rahbar N, Salehnezhad Z, Hatamie A, Babapour A. Graphitic carbon nitride nanosheets as a fluorescent probe for chromium speciation. *Microchim Acta* 2018;185:101.
- [88] Gao JW, Xiong HW, Zhang W, Wang Y, Wang HX, Wen W, et al. Electrochemiluminescent aptasensor based on beta-cyclodextrin/graphitic carbon nitride composite for highly selective and ultrasensitive assay of platelet derived growth factor BB. *Carbon* 2018;130:416–23.
- [89] Cheng Y, Nie J, Li Z, Yan Z, Xu G, Li H, et al. A molecularly imprinted polymer synthesized using β -cyclodextrin as the monomer for the efficient recognition of forchlorfenuron in fruits. *Anal Bioanal Chem* 2017;409:5065–72.
- [90] Shi J, Li G, Cui Y, Zhang Y, Liu D, Shi Y, et al. Surface-imprinted β -cyclodextrin-functionalized carbon nitride nanosheets for fluorometric determination of sterigmatocystin. *Microchim Acta* 2019;186:808.
- [91] Yaseen T, Pu H, Sun DW. Functionalization techniques for improving SERS substrates and their applications in food safety evaluation: a review of recent research trends. *Trends Food Sci Technol* 2018;72:162–74.
- [92] Martínez L, He L. Detection of mycotoxins in food using surface-enhanced Raman spectroscopy: a review. *ACS Appl Bio Mater* 2021;4:295–310.
- [93] Lee HK, Lee YH, Koh CSL, Phan-Quang GC, Han X, Lay CL, et al. Designing surface-enhanced Raman scattering (SERS) platforms beyond hotspot engineering emerging opportunities in analyte manipulations and hybrid materials. *Chem Soc Rev* 2018;48:731–56.
- [94] Sridhar K, Inbaraj BS, Chen BH. An improved surface enhanced Raman spectroscopic method using a paper-based grape skin-gold nanoparticles/graphene oxide substrate for detection of rhodamine 6G in water and food. *Chemosphere* 2022;301:134702.
- [95] Langer J, Jimenez de Aberasturi D, Aizpurua J, Alvarez-Puebla RA, Auguie B, Baumberg JJ, et al. Present and future of surface-enhanced Raman scattering. *ACS Nano* 2020;14:28–117.
- [96] Santhosh NM, Shvalya V, Modic M, Hojnik N, Zavasnik J, Olenik J, et al. Label-free mycotoxin Raman identification by high-performing plasmonic vertical carbon nanostructures. *Small* 2021;17:2103677.
- [97] Radi AE, Eissa A, Wahdan T. Voltammetric behavior of mycotoxin zearalenone at a single walled carbon nanotube screen-printed electrode. *Anal Methods* 2019;11:4494–500.
- [98] Nasir MZM, Novotný F, Alduhaish O, Pumera M. 3D-printed electrodes for the detection of mycotoxins in food. *Electr Commun* 2020;115:106735.
- [99] Gevaerd A, Banks CE, Bergamini MF, Marcolino-Junior LH. Nanomodified screen-printed electrode for direct determination of aflatoxin B1 in malted barley samples. *Sens Actuators, B* 2020;307:127547.
- [100] Cao Y, Feng T, Xu J, Xue C. Recent advances of molecularly imprinted polymer-based sensors in the detection of food safety hazard factors. *Biosens Bioelectron* 2019;141:111447.
- [101] Li W, Diao K, Qiu D, Zeng Y, Tang K, Zhu Y, et al. A highly-sensitive and selective antibody-like sensor based on molecularly imprinted poly(L-arginine) on COOH-MWCNTs for electrochemical recognition and detection of deoxynivalenol. *Food Chem* 2021;350:129229.